Turun yliopisto
University of Turku

BEYOND THE COSMOLOGICAL PRINCIPLE

Peter Sundell

TURUN YLIOPISTON JULKAISUJA – ANNALES UNIVERSITATIS TURKUENSIS
Sarja - ser. A I osa - tom. 545 | Astronomica - Chemica - Physica - Mathematica | Turku 2016

University of Turku

Faculty of Mathematics and Natural Sciences
Department of Physics and Astronomys

Supervised by

Iiro Vilja
University Lecturer
Department of Physics and Astronomy
University of Turku
Finland

Reviewed by

Juan García-Bellido
Associate Professor
Instituto de Física Teórica
Universidad Autónoma de Madrid
Spain

Krzysztof Bolejko
Senior Lecturer
School of Physics
The University of Sydney
Australia

Opponent

Kari Enqvist
Professor
Department of Physics
University of Helsinki
Finland

The originality of this thesis has been checked in accordance with the University of Turku quality assurance system using the Turnitin OriginalityCheck service.

ISBN 978-951-29-6564-9 (PRINT)
ISBN 978-951-29-6565-6 (PDF)
ISSN 0082-7002 (Print)
ISSN 2343-3175 (Online)
Painosalama Oy - Turku, Finland 2016

Acknowledgements

I am immensely grateful to my supervisor Iiro Vilja for guidance, patience, and countless hours of discussions, which eventually lead to the completion of this book. I am also grateful to Edvard Mörtsell and Tomi Koivisto for their contributions and guidance during my path. I thank my pre-examinators, Juan García-Bellido and Krzysztof Bolejko for their fair and useful comments on the manuscript of the book.

The people in the theoretical physics lab in the University of Turku is to thank for the good spirit, energy, and help. My friends outside the lab, thank you for all the moments outside physics counterbalancing the research.

From the bottom of my heart, I want to thank my family. In particular my parents, Kaj and Raili, who have supported me throughout my life in every possible way. I am also grateful to my wife, Johanna, who supported me through the book writing process and understood the long days and late hours in the past year.

I thank Magnus Ehrnrooth Foundation, Vilho, Yrjö and Kalle Väisälä Foundation, Nordita, and UTUGS for the financial support.

Contents

Abstract

Simplifying the Einstein field equation by assuming the cosmological principle yields a set of differential equations which governs the dynamics of the universe as described in the cosmological standard model. The cosmological principle assumes the space appears the same everywhere and in every direction and moreover, the principle has earned its position as a fundamental assumption in cosmology by being compatible with the observations of the 20th century. It was not until the current century when observations in cosmological scales showed significant deviation from isotropy and homogeneity implying the violation of the principle. Among these observations are the inconsistency between local and non-local Hubble parameter evaluations, baryon acoustic features of the Lyman-α forest and the anomalies of the cosmic microwave background radiation. As a consequence, cosmological models beyond the cosmological principle have been studied vastly; after all, the principle is a hypothesis and as such should frequently be tested as any other assumption in physics.

In this thesis, the effects of inhomogeneity and anisotropy, arising as a consequence of discarding the cosmological principle, is investigated. The geometry and matter content of the universe becomes more cumbersome and the resulting effects on the Einstein field equation is introduced. The cosmological standard model and its issues, both fundamental and observational are presented. Particular interest is given to the local Hubble parameter, supernova explosion, baryon acoustic oscillation, and cosmic microwave background observations and the cosmological constant problems. Explored and proposed resolutions emerging by violating the cosmological principle are reviewed. This thesis is concluded by a summary and outlook of the included research papers.

Tiivistelmä

Kosmologinen periaate, jonka otaksutaan pätevän kosmologisessa standardimallissa, olettaa avaruuden näyttävän samalta joka pisteessä ja joka suunnassa. Tämä periaate on ansainnut paikkansa hyvänä oletuksena sopimalla havaintoihin erittäin hyvin aina 2000-luvun vaihteeseen asti sekä yksinkertaistamalla Einsteinin yhtälön kauniiseen ja yksinkertaiseen muotoon. Vasta vuosituhannen vaihteen jälkeen tehdyissä havainnoissa on löytynyt uskottavia todisteita kosmologista periaatetta vastaan. Tällaisia havaintoja ovat muun muassa ristiriitaiset tulokset Hubblen parametrin määrityksessä, Lyman-α-metsän baryoniakustiset oskillaatiot sekä anomaliat kosmisessa taustasäteilyssä. Lisäksi, vaikka havaintoja kosmologista periaatetta vastaan ei olisikaan vielä löytynyt, periaatetta tulee testata kuin mitä tahansa oletusta fysiikassa.

Tässä väitöskirjassa tutkitaan ilmiöitä, jotka seuraavat kosmologisen periaatteen hylkäämisestä. Yleisellä tasolla voidaan sanoa, että periaatteesta luovuttaessa universumin geometria monimutkaistuu ja materiasisältö monimuotoistuu. Tämän seurauksena systeemiä kuvaavien yhtälöiden ratkaiseminen hankaloituu, joka tässä kirjassa havainnollistetaan esittelemällä kosmologinen standardimalli sekä joitakin kosmologista periaatetta rikkovia malleja. Myös kosmologisen standardimallin ongelmia havainnollistetaan konkreettisesti. Erityistä huomiota saavat Hubblen parametri, supernovat, baryoniakustiset oskillaatiot, kosminen taustasäteily sekä pimeän energian ongelma. Kosmologista periaatetta rikkovia malleja on tutkittu laajasti yrittäen löytää niistä ratkaisu kosmologisen standardimallin ongelmiin; näitä ratkaisuyrityksiä kuvaillaan. Lopuksi väitöskirjassa esitellyistä artikkeleista tehdään yhteenveto.

List of papers

This thesis consists of a review of the subject and the following original research articles [1, 2, 3, 4]:

I **Inhomogeneous cosmological models and fine-tuning of the initial state**,
P. Sundell and I. Vilja, Mod. Phys. Lett. **A29**, 1450053 (2014).

II **Can a void mimic the Λ in ΛCDM?**,
P. Sundell, E. Mörtsell and I. Vilja, JCAP **1508**, 037 (2015).

III **Anisotropic cosmology and inflation from a tilted Bianchi IX model**,
P. Sundell and T. Koivisto, Phys. Rev. **D92**, 123529 (2015).

IV **Inhomogeneity of the ΛLTB models**,
P. Sundell and I. Vilja, [arXiv:1601.05256].

Chapter 1

Introduction

It was 101 years ago, in 1915, when Albert Einstein provided his theory on gravity, known as general relativity. In cosmological scales, the theory has persisted as the most graceful and beautiful description of gravity. By this I mean that it is the simplest theory accurately capable confronting cosmological observations.

In 1917 general relativity was applied to cosmology for the first time, this was done by Einstein himself in Ref. [5] (see [6] for the English translation). In this paper, he introduced his view on our universe by presenting a static and finite model complying with the cosmological principle. In order to achieve this he had to introduce the cosmological constant to his equations; a constant that was not originally present in general relativity. We have to keep in mind that in those days the cosmological observations were far from that they are today and Einstein's static world view was actually supported by the fact that stars appear quite immobile in the sky. Let me add that Einstein's world view was actually quite progressive as for example Herschels's universe, where the universe is heliocentric, was still vital at the time [7].

General relativity inspired other physicists to construct alternative views of our universe too: in 1917 Willem de Sitter constructed an alternative static model in Ref. [8] and in 1922 and 1924 Alexander Friedmann introduced the radical idea that the universe might not be static [9, 10], respectively. However, Einstein did not recognise these models physically viable as de Sitter's model contained no ordinary matter and Friedmann's models were non-static [11].

First evidence against Einstein's static universe arose in the 1920's when the redshifts of some distant galaxies were measured; the static models were not ruled out, but favoured de Sitter's model over Einstein's model [11].

However, Einstein's model remained also viable as long as the redshifts are interpreted being caused by "the normal movement" (or the peculiar motion) of the galaxies [7]. Georges Lemaître gave an alternative interpretation in 1927 (an English translation is given in [12]) for the measured redshifts by utilising the expansion of the universe instead of peculiar velocities. His interpretation was not well accepted by the community of the physicist; the general opinion was well reflected by Einstein's comment on the model "from the physical point of view, that appeared completely abominable" [11].

In 1929 Edwin Hubble published his famous paper [13], where he gave a linear fit to his velocity-distance data of galaxies, nowadays known as Hubble's law. The results of Hubble's paper were not favourable for the static models but fitted well to Lemaître's expanding model, in fact, in his 1927 paper Lemaître presented Hubble's law before Hubble. Hubble's paper together with the discovered instability in the Einstein's static universe dealt a dead blow to the static models and lead to the acceptance of the expanding universes [11, 7]. However, the static models left their imprints on the model development. The ideology in the static models that the universe has always been and always will be as it is now kept on and resulted in e.g. the steady state model, where the universe expands but creates matter continuously in order to keep the matter density of the universe constant.

Lemaître saw things in a different light. In a series of papers (see [11]), he proposed and developed a universe that started from a much smaller and denser state than seen today and has expanded since. Fred Hoyle, a supporter of the steady state model, even ridiculed Lemaître for his model by calling him "the big bang man" [11], as if the universe was born is some big explosion. This name-calling eventually resulted in a name for Lemaître's model that is still in use, the big bang model. Despite of the rivals, the big bang model gathered also advocates and was further developed by several physicists. Gamow, Alpher and Hermann, for example, predicted that the big bang model should produce a blackbody radiation that would be observed today at ~ 5 K temperature [11, 14]. This prediction turned out particularly important as the detection of ~ 3.5 K isotropic excess antenna temperature in 1965 by Penzias and Wilson [15] gave the death sentence for the steady state models and established the big bang model.

The big bang model has been developed since and the version giving the best concordance between the model and observations today is called the

ΛCDM model. A notable fact in the above given historical review is that the most popular cosmological model based on general relativity, starting from Einstein's static model to the presently favoured ΛCDM model, has always relayed on the cosmological principle. For the very first models, this was justifiable due to the simplicity and beauty of the principle and the lack of observations. Today, the ΛCDM model can be justified by its simplicity, beauty and its remarkable compatibility with observations and phenomena. However, there is also evidence piling up against the ΛCDM model, like there was evidence piling up against the static and steady state models. If we were to learn anything about history, it would be that we should not reject alternatives due to our stubbornness and adherence to old norms.

Indeed, the lesson has been learned as many alternatives to the ΛCDM model are under active investigation, like the dark energy models and the models violating the cosmological principle. Put simply, the cosmological principle means that space looks the same everywhere and in every direction, and in more technical terms, space is homogeneous and isotropic at every point in space. Beauty and simplicity have always been cherished amongst the physicists, but on the other hand, beauty is in the eye of the beholder. The cosmological principle is usually assumed to hold in the dark energy models, which means that the mathematics of the models remains simple and beautiful. On the other hand, dark energy is often not needed when studying the inhomogeneous models, which implies the physical side of the model remains simple and beautiful. Then again, it might turn out that we have to discard the simplicity and beauty aspects and describe our universe with an ugly inhomogeneous dark energy model. After a long enough period of time, I am confident that someone will present the new theory in an elegant form, hence making it simple and beautiful again.

Papers [1, 2, 3, 4] are devoted to the study of whether relaxing the cosmological principle can resolve the paradigms of the concordance ΛCDM model. In particular, the effects of radial inhomogeneity have been investigated the dark energy problem in mind. In addition, the anisotropic evolution of the universe has been explored in order to gain understanding about the anomalies in the cosmic microwave background.

The thesis is organised as follows. Features of the Einstein field equation are covered in Chapter 2. A particular emphasis is laid on the geometrical properties, fluid properties and methods on solving the equations. In addition, some solutions are presented. Outlines of the cosmological standard

model are introduced in Chapter 3. In particular, features and observational aspects, relevant in the light of papers [1, 2, 3, 4], are scrutinized. Paradigms of the cosmological standard model are reviewed in Chapter 4, issues related to the aforementioned papers are stressed. Moreover, suggested and studied resolutions to these paradigms arising by violating the cosmological principle are contemplated. Chapter 5 is devoted to give a summary and outlook of the research papers.

Chapter 2

Einstein's theory of gravitation

Electromagnetism and gravity are the only forces effectively present in our everyday lives, other forces are negligible due to the large size of the "human" scales. Most astrophysical objects appear electrically neutral, hence it is justified to approximate that the cosmic scales are dominated by gravity. With these assumptions and approximations, a theory of gravity sufficiently describes the universe, in particular, the dynamics of the universe.

I consider Einstein's general relativity as the theory of gravitation. In this chapter, the theory is presented in the extent that is relevant to this work. More details can be found in various books and lecture notes, like Refs. [16, 17, 18, 19, 20]. Within the framework of general relativity, the dynamics are given by the Einstein field equation[1]

$$G_{ab} + \Lambda g_{ab} = \kappa T_{ab}. \tag{2.1}$$

Broadly speaking, this equation describes the interplay between geometry (G_{ab}) and matter (T_{ab}), but the meaning of the components G_{ab} and T_{ab} are presented in more detail in this chapter. In addition, the Einstein field equation contains the coupling constant κ and the cosmological constant, Λ, of which significance is discussed in the later chapters. The coupling constant $\kappa = 8\pi G$, where G is the Newtonian gravitation constant, describes the strength of the interplay between the gravity and matter. Throughout this introduction, I shall use the units where $8\pi G = 1$.

[1]The derivation of the Einstein field equation is given e.g. in [16] and [18].

2.1 Geometrical properties

2.1.1 Vectors, 1-forms and tensors

In general relativity, the space-time is a four-dimensional differentiable manifold which can locally be expressed by a coordinate system. Consequently, the vector fields are also four-dimensional and they are referred to as four-vectors (or vectors for short). Each vector is associated with a fixed point in space-time, p, and the set of vectors associated with the point p is the tangent space at p, which is denoted by T_p. A vector field is a set of vectors where there is only one vector at each point of the space-time. A parametric curve which is tangential to a vector field at each point is called an integral curve and the set of integral curves (of a vector field) is the congruence of curves. A basis of vector fields $\{\mathbf{e}_a\}$, where $a = 0, 1, 2, 3$, is a linearly independent set of vectors that spans a vector space. Therefore, any vector field $\mathbf{X}$ can be given as the linear combination

$$\mathbf{X} = X^a \mathbf{e}_a, \tag{2.2}$$

where X^a are the components of the vector field $\mathbf{X}$. I have used here the Einstein summation convention and shall use it throughout the book.

A vector space has a dual vector space which maps all objects from the vector space to real numbers. In particular, a vector basis $\{\mathbf{e}_a\}$ has the dual basis called 1-forms $\{\omega^a\}$ so that when a 1-form operates on a vector field (or vice versa), one has

$$\omega^a(\mathbf{e}_b) = \delta^a_b, \tag{2.3}$$

where δ^a_b is the Kronecker delta. Every dual vector ω can be written as

$$\omega = \hat{\omega}_a \omega^a, \tag{2.4}$$

where $\hat{\omega}_a$ are the components of the dual vector field ω.

Tensors $\mathbf{T}$ are constructed from vectors and 1-forms so that the basis of the tensor space is provided by a tensor product of the bases of the vectors and 1-forms. Tensors of type (p, q) are constructed from p vectors and q 1-forms. Consequently, vectors are type $(1, 0)$ tensors, 1-forms are type $(0, 1)$ tensors and scalars are type $(0, 0)$ tensors. An important tensor is

the metric tensor $\mathbf{g} = \mathbf{g}(\mathbf{e}_a, \mathbf{e}_b)$, which gives the line-element

$$ds^2 = g_{ab}\omega^a\omega^b, \tag{2.5}$$

where $\{\omega^a\}$ is the dual basis of a vector field basis $\{\mathbf{e}_a\}$. I consider only pseudo-Riemannian metric which is symmetric and indefinite. Brackets () are used to denote the symmetric indices and brackets [] to denote the antisymmetric indices in a tensor, e.g. $T_{(ab)} = (T_{ab} + T_{ba})/2$ and $T_{[ab]} = (T_{ab} - T_{ba})/2$.

The basis can always be chosen according to the situation. Frequently, it is convenient to choose the basis $\{\mathbf{e}_a\}$ to be a coordinate basis[2] $\{\partial/\partial x^a\}$ which dictates the dual basis to be the coordinate 1-forms $\{dx^a\}$. The abbreviation $\{\partial x_a\} = \{\partial/\partial x^a\}$ is employed. As a consequence of Eq. (2.2), the general basis and its dual can be given with respect to a coordinate basis and its dual:

$$\mathbf{e}_a = \mathbf{e}_a^b\partial_b, \quad \omega^a = \omega_b^a dx^b. \tag{2.6}$$

The line-element (2.5) in terms of a coordinate basis and its dual is

$$ds^2 = g_{ab}dx^a dx^b, \tag{2.7}$$

where $g_{ab} = \mathbf{g}(\partial_a, \partial_b)$. Another commonly used basis is the so-called orthonormal frame, where the vectors $\mathbf{e}_a$ are of unit length, orthogonal to each other, and $\mathbf{e}_0$ is time-like, hence one can write

$$\mathbf{g}(\mathbf{e}_a\mathbf{e}_b) = \eta_{ab}, \tag{2.8}$$

where η_{ab} is the Minkowski metric with one negative component. The line-element (2.5) in terms of an orthonormal basis and its dual is

$$ds^2 = \eta_{ab}\omega^a\omega^b. \tag{2.9}$$

[2] A common practice is to label a coordinate basis using different characters than is used to label a general basis in order to facilitate reading. I do not follow the practice here, because it would lead to a notation that is inconsistent with the notation in papers [1, 2, 3, 4]. Nevertheless, the notation used here should not lead to misconceptions as I merely introduce some other bases and work only in a coordinate basis.

2.1.2 Connection

In order to compare vectors in T_p and T_q, $p \neq q$, one needs to know how the tangent spaces are connected with each other. This can be described with the connection operator ∇. A connection on space-time maps two vector fields $\mathbf{X}$, $\mathbf{Y}$ to a vector field $\mathbf{Z}$: $\nabla(\mathbf{X}, \mathbf{Y}) \equiv \nabla_{\mathbf{X}}\mathbf{Y} = \mathbf{Z}$. Furthermore, it is a linear map with respect to the first argument, additive with respect to the second argument, and comply with Leibnitz's rule of differentiation:

$$\begin{aligned} \nabla_{f\mathbf{X}+\mathbf{Y}}\mathbf{Z} &= f\nabla_{\mathbf{X}}\mathbf{Z} + \nabla_{\mathbf{Y}}\mathbf{Z} \\ \nabla_{\mathbf{X}}(\mathbf{Y}+\mathbf{Z}) &= \nabla_{\mathbf{X}}\mathbf{Y} + \nabla_{\mathbf{X}}\mathbf{Z} \\ \nabla_{\mathbf{X}}(f\mathbf{Y}) &= (\nabla_{\mathbf{X}}f)\mathbf{Y} + f\nabla_{\mathbf{X}}(\mathbf{Y}) \end{aligned} \tag{2.10}$$

where f is a scalar function and

$$\nabla_{\mathbf{X}} f = \mathbf{X}f. \tag{2.11}$$

The connection coefficients $\Gamma^c{}_{ab}$ are defined through the relation

$$\nabla_{\mathbf{e}_b}\mathbf{e}_a = \Gamma^c{}_{ab}\mathbf{e}_c. \tag{2.12}$$

Employing Eqs. (2.6), (2.10), (2.11), and (2.12) one finds the covariant derivative for a vector field $\mathbf{X}$:

$$\nabla_{\mathbf{e}_a}\mathbf{X} = (\mathbf{e}_a{}^i\partial_i X^b)\mathbf{e}_b + X^b\Gamma^c{}_{ba}\mathbf{e}_c, \tag{2.13}$$

which after some index manipulation yields the component form

$$\nabla_{\mathbf{e}_a}X^b = \mathbf{e}_a{}^i\partial_i(X^b) + X^c\Gamma^b{}_{ca}, \tag{2.14}$$

where the abbreviation $\nabla_{\mathbf{e}_a}X^b = (\nabla_{\mathbf{e}_a}X)^b$ has been used. Applying Eq. (2.3) to any vector and its dual vector results in a scalar: $\mathbf{V}(\omega) = V^a\hat{\omega}_a$. Operating on the obtained scalar with the connection operator and employing Eqs. (2.3), (2.11) and (2.14), one arrives with an expression that determines how the connection operates on 1-forms:

$$\mathbf{e}_a\nabla_{\mathbf{e}_b}\omega^c = -\Gamma^c{}_{ab}. \tag{2.15}$$

Furthermore, the result can be generalised to tensors and for example, the covariant derivative of a type $(1,1)$ tensor reads as

$$\nabla_{\mathbf{e}_c} T^a_{\ b} = \mathbf{e}_c(T^a_{\ b}) + \Gamma^a_{\ dc} T^d_{\ b} - \Gamma^d_{\ bc} T^a_{\ d}. \tag{2.16}$$

I shall sometimes follow the common practice that the covariant derivative is denoted by a semicolon. For example, in this notation, the covariant derivative of a type $(1,1)$ tensor with respect to $\mathbf{e}_c$ is $T^a_{\ b;c}$.

The commutator maps any two vector fields, $\mathbf{X}, \mathbf{Y}$, to a vector field $\mathbf{Z}$. In particular, if the vector fields are chosen to be components of a basis $\{\mathbf{e}_a\}$, the commutators define location dependent coefficients $\gamma^c_{\ ab} = \gamma^c_{\ ab}(x^j)$:

$$[\mathbf{e}_a, \mathbf{e}_b] = \gamma^c_{\ ab} \mathbf{e}_c. \tag{2.17}$$

The coefficients $\gamma^c_{\ ab}$ are knows as the commutation functions and the definition (2.17) clearly exhibits them to be antisymmetric with respect to the last two indices, $\gamma^a_{\ bc} = \gamma^a_{\ [bc]}$. The explicit forms of the commutation functions depend on the used basis, and for example, they are zero for a coordinate basis.

I take the connection to be the Levi-Civita connection, thus it is torsion-free

$$\nabla_{\mathbf{X}} \mathbf{Y} - \nabla_{\mathbf{Y}} \mathbf{X} = [\mathbf{X}, \mathbf{Y}], \tag{2.18}$$

and metric

$$\nabla \mathbf{g} = 0. \tag{2.19}$$

Now one can write an equation for $\Gamma^c_{\ ab}$ using the metric components and commutation functions and it is obtained as follows. Eqs. (2.12), (2.17) and (2.18) can be combined to give

$$\Gamma^c_{\ ab} = \Gamma^c_{\ ba} - \gamma^c_{\ ab} \tag{2.20}$$

The metric condition and the formula for the covariant derivative of a tensor yield

$$0 = \nabla_{\mathbf{e}_c} g_{ab} = \mathbf{e}_c(g_{ab}) - \Gamma^d_{\ ca} g_{db} + \gamma^d_{\ ac} g_{db} - \Gamma^d_{\ bc} g_{ad}. \tag{2.21}$$

where Eq. (2.20) is substituted in. Equivalently,

$$0 = \nabla_{\mathbf{e}_a} g_{bc} = \mathbf{e}_a(g_{bc}) - \Gamma^d{}_{ab} g_{dc} + \gamma^d{}_{ba} g_{dc} - \Gamma^d{}_{ca} g_{bd}, \quad (2.22)$$

$$0 = \nabla_{\mathbf{e}_b} g_{ca} = \mathbf{e}_b(g_{ca}) - \Gamma^d{}_{bc} g_{da} + \gamma^d{}_{cb} g_{da} - \Gamma^d{}_{ab} g_{cd}. \quad (2.23)$$

Adding Eqs. (2.21) and (2.23) together and then subtracting Eq. (2.22) from the obtained equation yields

$$\Gamma_{abc} = \frac{1}{2}[\mathbf{e}_b(g_{ca}) + \mathbf{e}_c(g_{ab}) - \mathbf{e}_a(g_{bc}) + \gamma^d{}_{cb} g_{da} + \gamma^d{}_{ac} g_{db} - \gamma^d{}_{ba} g_{dc}], \quad (2.24)$$

where $\Gamma_{abc} = g_{ad}\Gamma^d{}_{bc}$.

2.1.3 Space-time curvature

The curvature of the space-time is characterised by the Riemann tensor $\mathbf{R}(\mathbf{X}, \mathbf{Y})$, which is defined through

$$\mathbf{R}(\mathbf{X}, \mathbf{Y})\mathbf{Z} = \nabla_{\mathbf{X}} \nabla_{\mathbf{Y}} \mathbf{Z} - \nabla_{\mathbf{Y}} \nabla_{\mathbf{X}} \mathbf{Z} - \nabla_{[\mathbf{X},\mathbf{Y}]} \mathbf{Z} \quad (2.25)$$

for any vector fields $\mathbf{X}$, $\mathbf{Y}$ and $\mathbf{Z}$. By setting $\mathbf{X} = \mathbf{e}_c$, $\mathbf{Y} = \mathbf{e}_d$ and $\mathbf{Z} = \mathbf{e}_b$,

$$\mathbf{R}(\mathbf{e}_c, \mathbf{e}_d)\mathbf{e}_b = \nabla_{\mathbf{e}_c} \nabla_{\mathbf{e}_d} \mathbf{e}_b - \nabla_{\mathbf{e}_d} \nabla_{\mathbf{e}_c} \mathbf{e}_b - \nabla_{[\mathbf{e}_c,\mathbf{e}_d]} \mathbf{e}_b, \quad (2.26)$$

and by applying Eqs. (2.10), (2.11), (2.12) and (2.17) the Riemann tensor can be expressed in terms of the commutator functions, connection coefficients and a basis $\{\mathbf{e}_a\}$:

$$\begin{aligned} \mathbf{R}(\mathbf{e}_c, \mathbf{e}_d)\mathbf{e}_b &= \nabla_{\mathbf{e}_c} \Gamma^a{}_{bd} \mathbf{e}_a - \nabla_{\mathbf{e}_d} \Gamma^a{}_{bc} \mathbf{e}_a - \nabla_{\gamma^a{}_{cd} \mathbf{e}_a} \mathbf{e}_b \\ &= \mathbf{e}_c(\Gamma^a{}_{bd})\mathbf{e}_a - \mathbf{e}_d(\Gamma^a{}_{bc})\mathbf{e}_a \\ &\quad + \Gamma^a{}_{bd}\Gamma^e{}_{ac}\mathbf{e}_e - \Gamma^a{}_{bc}\Gamma^e{}_{ad}\mathbf{e}_e - \gamma^a{}_{cd}\Gamma^e{}_{ba}\mathbf{e}_e. \end{aligned} \quad (2.27)$$

The components of the Riemann tensor $R^a{}_{bcd}\mathbf{e}_a$ becomes defined by setting

$$\mathbf{R}(\mathbf{e}_c, \mathbf{e}_d)\mathbf{e}_b = R^a{}_{bcd}\mathbf{e}_a, \quad (2.28)$$

yielding

$$R^a{}_{bcd} = \mathbf{e}_c(\Gamma^a{}_{bd}) - \mathbf{e}_d(\Gamma^a{}_{bc}) + \Gamma^e{}_{bd}\Gamma^a{}_{ec} - \Gamma^e{}_{bc}\Gamma^a{}_{ed} - \gamma^e{}_{cd}\Gamma^a{}_{be}. \quad (2.29)$$

Because the commutation functions (2.17) are antisymmetric with respect to the last two indices, $\gamma^a{}_{bc} = \gamma^a{}_{[bc]}$, one can readily see that the components of the Riemann tensor are also antisymmetric with respect to the last two indices

$$R^a{}_{bcd} = R^a{}_{b[cd]}. \tag{2.30}$$

Evaluating the Riemann tensor in a coordinate basis, a straightforward calculation shows that the Riemann tensor satisfy also the so-called Jacobi identity:

$$R^a{}_{[bcd]} = 0. \tag{2.31}$$

In a coordinate basis it is also evident that the Riemann tensor obey the Ricci identity

$$X^a{}_{;dc} - X^a{}_{;cd} = R^a{}_{bcd} X^b, \tag{2.32}$$

and the Bianchi identity

$$0 = R^a{}_{b[cd;e]}. \tag{2.33}$$

These are all tensor identities and therefore hold in any basis.

In a space-time where the metric is pseudo-Riemannian and the connection is the Levi-Civita connection, the underlying manifold is a pseudo-Riemannian manifold. Consequently, the Riemann tensor possesses further symmetries. The simplest way to find them is in Riemann normal coordinates, where the basis is a coordinate basis and locally $\Gamma^a{}_{bc} = 0$ for all a, b, c running from 0 to 3. Now, the metric condition (2.19) implies $\partial_a g_{bc} = 0$ locally. The connection coefficients vanish in these coordinates and the Riemann tensor ($R_{a'bcd} = g_{a'a} R^a{}_{bcd}$) assumes the form

$$R_{a'bcd} = g_{a'a} \left[\partial_c (\Gamma^a{}_{bd}) - \partial_d (\Gamma^a{}_{bc}) \right]. \tag{2.34}$$

This can be further reduced by substituting Eq. (2.24) in and employing the condition $\partial_a g_{bc} = 0$, yielding

$$R_{a'bcd} = \frac{1}{2} \left[\partial_c \partial_b g_{a'd} - \partial_c \partial_{a'} g_{db} - \partial_d \partial_b g_{a'c} + \partial_d \partial_{a'} g_{cb} \right]. \tag{2.35}$$

Because the metric tensor is symmetric with respect to its indices and the partial derivatives commute, the right side of the above expression reveals that

$$R_{abcd} = R_{[ab]cd}, \tag{2.36}$$
$$R_{abcd} = R_{cdab}. \tag{2.37}$$

These equations hold in any basis as they are tensor identities.

In general, the Riemann tensor R_{abcd} has n^4 components in n-dimensional space-time. Taking into account the symmetries given in Eqs. (2.30) and (2.36), the remaining number of independent components is $[n(n-1)/2]^2$ ($[n(n-1)/2]$ for the pair a and b and the same number for the pair c and d). The independent components of these pairs can be rearranged into a $[n(n-1)/2] \times [n(n-1)/2]$ matrix, which is symmetric according to Eq. (2.37) and therefore consisting of $(n^4 - 2n^3 + 3n^2 - 2n - 1)/8$ independent components. Finally, the Jacobi identity introduces $[d(d-1)(d-2)(d-3)]/4!$ new constraining equations and hence the number of independent components in the four-dimensional Riemann tensor is 20.

By defining the Ricci tensor as

$$R_{bd} \equiv R^{a}{}_{bad}, \tag{2.38}$$

and furthermore the Ricci scalar as

$$R \equiv R^{a}{}_{a}, \tag{2.39}$$

one can finally present the definition for the Einstein tensor introduced in Eq. (2.1):

$$G_{ab} \equiv R_{ab} - \frac{1}{2} R g_{ab}. \tag{2.40}$$

As the Ricci tensor and metric tensor are symmetric in their indices, so is the Einstein tensor, hence having 10 independent components.

The Riemann tensor has 20 independent components, but as a symmetric tensor the Ricci tensor has only 10 independent components; the missing 10 independent components are in the Weyl tensor

$$C^{ab}{}_{cd} = R^{ab}{}_{cd} - 2\delta^{[a}_{\ [c} R^{b]}_{\ d]} + \frac{1}{3} R 2\delta^{a}{}_{[c}\delta^{b}{}_{d]}. \tag{2.41}$$

However, as the metric tensor consists of ten independent components and the Einstein field equation includes 10 independent equations, the metric components can be solved from the Einstein field equation (modulo boundary conditions). Moreover, as all components of the Riemann tensor can be presented with respect to the metric and its derivatives, the components of the Weyl tensor can be presented this way too. Consequently, the Weyl tensor cannot bring additional information in the system, but can merely act as convenient tools at some cases. The Weyl tensor possesses the symmetries

$$C_{abcd} = C_{cdab} = C_{[ab][cd]}, \quad C_{a[bcd]} = 0, \quad C^{a}{}_{bad} = 0. \tag{2.42}$$

The Weyl tensor is a conformal tensor as it remains invariant under conformal transformations. This implies that C_{abcd} describes non-local gravitational effects. In analog to the electromagnetic field tensor, the Weyl tensor is associated with its electric part E_{ab} and magnetic part H_{ab} with respect to the four-velocity u^a, which will be defined in Section 2.2.1:

$$E_{ab} = C_{abcd}u^b u^d, \quad H_{ab} = {}^*C_{abcd}u^b u^d, \tag{2.43}$$

where

$${}^*C_{abcd} = \frac{1}{2}\eta_{ab}{}^{st}C_{stcd}. \tag{2.44}$$

The Levi-Civita symbol ϵ^{abcd}, which is antisymmetric with respect to every index and $\epsilon^{0123} = 1$, defines the antisymmetric tensor

$$\eta^{abcd} = \frac{1}{\sqrt{-g}}\epsilon^{abcd}, \tag{2.45}$$

where g is the determinant of the metric tensor.

The Bianchi identity (2.33) leads to the conservation of the covariant derivative of the Einstein tensor,

$$G^{ab}{}_{;b} = 0, \tag{2.46}$$

introducing four additional equations in four-dimensional space-time.

The choice of a basis has a substantial effect on the Riemann tensor, and consequently on the Einstein tensor. In an orthonormal basis, the metric

takes Minkowskian form and hence the connection components (2.12) do not depend on the derivatives of the metric. Consequently, the components of the Riemann tensor (2.28) depend on the commutation functions $\gamma^c{}_{ab}$ and their first order derivatives $\mathbf{e}_d\gamma^c{}_{ab}$. On the other hand, in a coordinate basis the commutation functions vanish and the connection components (2.12) do depend on the derivatives of the metric. As a consequence, the components of the Riemann tensor (2.28) depend on the components of the metric, g_{ab}, and its first and second order derivatives, $\partial_c g_{ab}$ and $\partial_d\partial_c g_{ab}$, respectively. That is, the choice of the basis affects the order of the Einstein field equation: the coordinate basis yields second order differential equations whereas the orthonormal frame yields first order differential equations.

2.1.4 Killing vectors and space-time symmetry

The Lie derivative can be considered dragging objects along any congruence of curves and hence is a mapping of a manifold into itself. The Lie derivative with respect to a vector field $\mathbf{X}$ is denoted by $\mathcal{L}_\mathbf{X}$. If

$$\mathcal{L}_\mathbf{X} g_{ab} = 0, \tag{2.47}$$

the metric remains invariant when dragged along any congruence stipulated by the vector field $\mathbf{X}$ and $\mathcal{L}_\mathbf{X}$ is an isometry. Eq. (2.47) can be equivalently written as

$$\mathbf{X}_{a;b} - \mathbf{X}_{b;a} = 0, \tag{2.48}$$

which is known as the Killing equation and a vector field $\mathbf{X}$ satisfying the Killing equation is a Killing vector field. The set of all Killing vector fields forms a Lie algebra and if its basis is denoted by $\{\xi_A\}$, where $A = 1, 2, \ldots, r$ and r is the dimension of the algebra, one has

$$[\xi_A, \xi_B] = C^C{}_{AB}\xi_C. \tag{2.49}$$

The structure constants of the algebra $C^C{}_{AB}$ are antisymmetric with respect to the two lower indices.

The set of the isometries of a manifold generated by $\{\xi_A\}$ forms the corresponding r dimensional Lie group G_r. The elements of G_r defines orbits on a manifold: the set of points where the elements of G_r maps a fixed point $p \in M$ is called the orbit of a point p under the group G_r. There

can be orbits of different dimensions, but they cannot exceed the dimension of the group r. In the case where the dimension of the orbit is equal to the dimension of the group G_r, the Killing vector fields $\{\xi_A\}$ are linearly independent at point p and the group is said to be simply transitive. If the dimension of the orbit is s and $s < r$, the Killing vector fields $\{\xi_A\}$ are linearly dependent at point p and the group is said to be multiply transitive. In the latter case, the Killing vector fields generate a subgroup of isometries of dimension d, so that

$$r = s + d, \tag{2.50}$$

and this subgroup is known as the isotropy subgroup of p. The isotropy subgroup of p leaves point p fixed thus describing local symmetries.

Cosmological models can be classified using these symmetry properties. An extensive classification is given in [19] and I shall only present here the scenarios relevant to this work. The dimension of the orbits, s, describes the homogeneity properties of the space-time, whereas the dimension of the isotropy subgroup, d, determines the isotropy properties of the space-time.

The case $s = 3$ corresponds to homogeneous three-dimensional orbits. If the orbits are space-like, three cosmologically interesting scenarios arise and they differ from each other by their dimension of isotropy subgroup d. For $d = 3$, the homogeneous space-like orbits are also isotropic and such space-time is used in the Friedmann models. For $d = 0$, the homogeneous space-like orbits contain no isotropy and such space-time is used in the Bianchi models. Locally rotationally symmetric (LRS) Bianchi models are obtained if $d = 1$.

Homogeneous two-dimensional orbits are obtained if $s = 2$. If the orbits are space-like and $d = 1$, the symmetry properties allow for the radially inhomogeneous Lemaître-Tolman-Bondi (LTB) models.

2.1.5 Hypersurfaces

Hypersurfaces are submanifolds of dimension $m - 1$ in a manifold of dimension m and one can always choose coordinates so that one of the coordinates remains constant on the family of non-intersecting hypersurfaces. In cosmology, it is often convenient to choose the coordinates so that time remains constant on the hypersurfaces, but this is not always the best foliation of the space-time and the coordinates should be chosen according to

the situation.

A time-like unit vector **u** satisfying the condition

$$u^a u_a = -1 \tag{2.51}$$

defines a projection tensor

$$h_{ab} = g_{ab} + u_a u_b, \tag{2.52}$$

which projects into the hypersurface orthogonal to vector **u**:

$$h_{ab}u^b = 0, \quad h_a{}^c h_c{}^d = h_a{}^d, \quad h_a{}^a = 3. \tag{2.53}$$

In the special case where the hypersurface orthogonal to **u** is constant in time (or spatial), I denote

$$u^a = n^a, \quad \hat{h}_{ab} = g_{ab} + n_a n_b. \tag{2.54}$$

and the line-element can be locally given in synchronous Gaussian normal coordinates:

$$ds^2 = -dt^2 + \hat{h}_{ij} d\tilde{x}^i d\tilde{x}^j, \tag{2.55}$$

where $\hat{h} = \hat{h}_{ij}(t, \tilde{\mathbf{x}})$ is the metric of the three-dimensional submanifold and $i, j = 1, 2, 3$ (I shall preserve indices $i, j, k, \ldots$ to label only the spatial components). That is, the metric can be foliated into spatial surfaces.

2.2 Matter content

2.2.1 Classical source

According to Einstein, the curvature of the space-time is sourced by the matter content of the universe. The matter content is described by the energy-momentum tensor T_{ab}, which can be decomposed with respect to the four-velocity u^a as

$$T_{ab} = \rho u_a u_b + p(g_{ab} + u_a u_b) + q_a u_b + u_a q_b + \pi_{ab}, \tag{2.56}$$

where ρ is the energy density, p is the pressure, q_a is the energy conduction, and π_{ab} is the anisotropic shear as measured by the observer moving

with the four-velocity u^a. These quantities are subject to the following constraints: q_a and π_{ab} are orthogonal to the four-velocity and π_{ab} is traceless and symmetric,

$$q_a u^a = 0, \quad \pi_{ab} u^a = 0, \quad \pi_a{}^a = 0, \quad \pi_{ab} = \pi_{ba}, \tag{2.57}$$

respectively. The four-velocity is defined as

$$u^a = \frac{dx^a}{d\tau} \quad \Rightarrow \quad u^a u_a = -1, \tag{2.58}$$

where $x^a = x^a(\tau)$ describes the world lines of the cosmic fluid in the local coordinates with respect to the proper time τ. The results given in Section 2.1.5 for the vector $\mathbf{u}$ applies to the four-velocity as it is a time-like unit vector satisfying Eq. (2.51). Moreover, the four-velocity assumes the form

$$u^a = \delta^a_0, \tag{2.59}$$

if the observer is comoving with the non-tilted fluid flow.

If the world lines are orthogonal to the hypersurfaces of constant time, or equivalently $\mathbf{n}$ is tangential to the world lines, the fluid flow is called non-tilted. The coordinate system of the observer comoving with non-tilted fluid can be written as in Eq. (2.55). On the other hand, if the world lines are not orthogonal to the hypersurfaces of constant time, or equivalently $\mathbf{n}$ is not tangential to the world lines, the fluid flow is called tilted. Now, the observer in the coordinate system (2.55) is not comoving with the tilted fluid and the four-velocity can be written as

$$u^a = \Gamma(n^a + v^a), \tag{2.60}$$

where v^a exhibit the velocity of the fluid in the observer's frame and

$$u^a v_a = 0, \quad \Gamma = (1 - v^2)^{-1/2}, \quad v^2 = v^a v_a. \tag{2.61}$$

Alternatively, a tilted four-velocity can be given with respect to the so-called tilting angle $\lambda(t)$. For example, in Ref. [3] the tilted four-velocity is written as

$$u^a = (\cosh[\lambda(t)], 0, 0, \sinh[\lambda(t)] e^{2\beta(t) - \alpha(t)}), \tag{2.62}$$

where $\alpha(t)$ and $\beta(t)$ are dynamical variables of the metric, introduced in Section 2.4.4. The relation between the variables of the two expressions is

$$\Gamma = \cosh[\lambda(t)], \quad v^1 = v^2 = 0, \quad v^3 = \frac{\sinh[\lambda(t)]}{\cosh[\lambda(t)]} e^{2\beta(t)-\alpha(t)}. \tag{2.63}$$

The interpretation of the fluid properties is not unambiguous, but dependent on the choice of the frame. For example, consider a observer comoving with tilted perfect fluid, where $q^a = \pi^{ab} = 0$ and the energy-momentum tensor reads as

$$T_{ab} = \rho u_a u_b + p(g_{ab} + u_a u_b). \tag{2.64}$$

Now, the four-velocity is (2.59) and ρ and p are respectively the matter density and pressure of the fluid as observed in the fluid frame. However, the four-velocity of the fluid assumes the form (2.60) for the observer in the coordinate system (2.55). Consequently, this observer experiences also the shear and the energy flux, because in this frame

$$\tilde{T}_{ab} = \tilde{\rho} n_a n_b + \tilde{p}(g_{ab} + n_a n_b) + \tilde{q}_a n_b + n_a \tilde{q}_b + \tilde{\pi}_{ab}, \tag{2.65}$$

where

$$\begin{aligned} \tilde{\rho} &= \rho + \Gamma^2 v^2(\rho + p), \\ \tilde{p} &= p + \frac{1}{3}\Gamma^2 v^2(\rho + p), \\ \tilde{q}_a &= \Gamma^2(\rho + p) v_a, \\ \tilde{\pi}_{ab} &= \Gamma^2(\rho + p)\left[v_a v_b - \frac{1}{3}\Gamma^2 v^2(\rho + p)\right], \end{aligned} \tag{2.66}$$

are respectively the energy density, the pressure, the energy conduction, and the trace-free anisotropic shear as experienced by this observer. Note that $\tilde{T}_{ab} = T_{ab}$ and tilde merely emphasises that the tensors are evaluated in different coordinate systems.

In cosmological context, the cosmic fluid is frequently assumed to comply with the equation of state

$$p = w\rho, \tag{2.67}$$

where the equation of state parameter w is constant. This assumption is

convenient when exploring the properties of a cosmic era where the dynamics is dominated by a single component. The most important eras are the cosmological constant, dust, and radiation dominated eras, which respectively correspond to w values -1, 0, and $1/3$.

Two approaches appear useful when studying phase transitions between eras. The quantities in the energy-momentum tensor (2.56) are considered as effective or the energy-momentum tensor (2.56) is assumed to be composed from components T^I_{ab} as

$$T_{ab} = \sum_I T^I_{ab}, \tag{2.68}$$

where the index I refers to different components of energy density, like dark energy, radiation, or dust. In general, each energy component has its own four-velocity u^I_a. It is convenient to give each u^I_a with respect to some chosen four-velocity, for example n_a, in which case each u^I_a and T^I_{ab} becomes decomposed as

$$u^I_a = \Gamma(n^I_a + v^I_a), \tag{2.69}$$

$$\tilde{T}^I_{ab} = \tilde{\rho}^I n_a n_b + \tilde{p}^I(g_{ab} + n_a n_b) + \tilde{q}^I_a n_b + n_a \tilde{q}^I_b + \tilde{\pi}^I_{ab}, \tag{2.70}$$

where $\tilde{\rho}^I$, $\tilde{p}^I$, $\tilde{q}^I_a$, and $\tilde{\pi}^I_{ab}$ are as in Eq. (2.66) only if T^I_{ab} is perfect fluid in its own frame; otherwise the expressions for $\tilde{\rho}^I$, $\tilde{p}^I$, $\tilde{q}^I_a$, and $\tilde{\pi}^I_{ab}$ are more cumbersome. Applying this to each energy component I and employing Eq. (2.68) yields

$$T_{ab} = \sum_I \tilde{T}^I_{ab} = \tilde{\rho} n_a n_b + \tilde{p}(g_{ab} + n_a n_b) + \tilde{q}_a n_b + n_a \tilde{q}_b + \tilde{\pi}_{ab} = \tilde{T}_{ab}, \tag{2.71}$$

where

$$\tilde{\rho} = \sum_I \tilde{\rho}^I, \quad \tilde{p} = \sum_I \tilde{p}^I, \quad \tilde{q}_a = \sum_I \tilde{q}^I_a, \quad \tilde{\pi}_{ab} = \sum_I \tilde{\pi}^I_{ab}, \tag{2.72}$$

and $\tilde{\rho}^I$, $\tilde{p}^I$, $\tilde{q}^I_a$, and $\tilde{\pi}^I_{ab}$ are respectively the energy density, the pressure, the energy conduction, and the shear of the energy component I as experienced by the observer in the coordinate system (2.55). Therefore $\tilde{\rho}$, $\tilde{p}$, $\tilde{q}_a$, and $\tilde{\pi}_{ab}$ are the corresponding effective quantities explicitly giving the connection between the effective energy-momentum tensor and its component decomposition in Eq. (2.68).

2.2.2 Conservation of energy and momentum

The Einstein field equation (2.1) together with the vanishing divergence of the Einstein tensor (2.46) yield four important conservation equations, the conservation of energy-momentum tensor:

$$\nabla_a T^{ab} = 0. \tag{2.73}$$

The energy-momentum tensor (2.56) is decomposed into parts parallel and orthogonal to the four-velocity of the fluid u^a. The component parallel to u^a gives the energy conservation equation,

$$\dot{\rho} = -3H(\rho + p) - h^a{}_b \nabla_a q^b - 2\dot{u}_a q^a - \sigma^a{}_b \pi^b{}_a, \tag{2.74}$$

and the components projected to the hypersurface h_{ab} result in three equations for the conservation of momentum,

$$\begin{aligned} h^a{}_b \dot{q}^b &= -4Hq^a - h^a{}_b \nabla^b p - (\rho + p)\dot{u}^a - h^a{}_c h^b{}_d \nabla_b \pi^{cd} \\ &\quad -\dot{u}_b \pi^{ab} - \sigma^a{}_b q^b + \eta^{abcd} \omega_b q_c u_d. \end{aligned} \tag{2.75}$$

2.2.3 Kinematical quantities and spatial curvature

The covariant derivative of the four-velocity can be decomposed into its irreducible parts:

$$u_{a;b} = \sigma_{ab} + \omega_{ab} + \frac{1}{3}\Theta h_{ab} - \dot{u}_a u_b, \tag{2.76}$$

where

$$\Theta = u^a{}_{;a}, \tag{2.77}$$

$$\dot{u}_a = u_{a;b} u^b, \tag{2.78}$$

$$\sigma_{ab} = u_{(a;b)} - \frac{1}{3}\Theta h_{ab} + \dot{u}_{(a} u_{b)}, \tag{2.79}$$

$$\omega_{ab} = u_{[a;b]} + \dot{u}_{[a} u_{b]}. \tag{2.80}$$

The scalar Θ describes the rate of volume expansion. Thus, by defining

$$H \equiv \frac{1}{3}\Theta, \tag{2.81}$$

H can be considered as a generalised Hubble scalar as it becomes the conventional Hubble scalar in isotropic and homogeneous space-times. The vector $\dot{u}^a$ is the relativistic acceleration vector induced by other forces than gravity; it vanishes for freely falling particles. The type $(0,2)$ tensor σ_{ab} is the so-called rate of shear tensor and it is trace-free, symmetric, and orthogonal to the four-velocity:

$$\sigma^a{}_a = 0, \quad \sigma_{ab} = \sigma_{(ab)}, \quad \sigma_{ab}u^b = 0. \tag{2.82}$$

The type $(0,2)$ tensor ω_{ab} describes the antisymmetric part of the covariant derivative of the four-velocity that is orthogonal to it,

$$\omega_{ab} = \omega_{[ab]}, \quad \omega_{ab}u^b = 0, \tag{2.83}$$

and is referred as the vorticity tensor.

It proves convenient to define the vorticity vector ω^a and the magnitudes of the above defined tensors. The vorticity vector is

$$\omega^a = \frac{1}{2}\eta^{abcd}u_b\omega_{[cd]}, \tag{2.84}$$

which is also orthogonal to the four-velocity $\omega^a u_a = 0$. The magnitudes of the vorticity ω, shear σ, and acceleration $\dot{u}$ are defined as

$$\omega = (\omega^a\omega_a)^{1/2} = \left(\frac{1}{2}\omega^{ab}\omega_{ab}\right)^{1/2}, \tag{2.85}$$

$$\sigma = \left(\frac{1}{2}\sigma^{ab}\sigma_{ab}\right)^{1/2}, \tag{2.86}$$

$$\dot{u} = (\dot{u}^a\dot{u}_a)^{1/2}. \tag{2.87}$$

The four-velocity is said to be irrotational, if the vorticity is zero.

For the metric $\hat{h}_{ij}(t,\tilde{\mathbf{x}})$, it is intuitively clear to define a curvature tensor analogous to Eq. (2.29). The three dimensional spatial curvature tensor is obtained from the four-dimensional by "removing" the time-components from it. Furthermore, as the four-dimensional Ricci scalar R was obtained from the four-dimensional curvature tensor, analogously, the three-dimensional Ricci scalar ${}^3R$ is obtained from the three-dimensional curva-

ture tensor by replacing g_{ab} by $\hat{h}_{ij}(t, \tilde{\mathbf{x}})$, yielding

$$ {}^3R = -\frac{2}{3}\Theta^2 + 2\sigma^2 + 2\rho + 2\Lambda. \tag{2.88} $$

The Einstein tensor, defined in (2.40), is essentially dependent on the metric components and/or the commutation functions and their derivatives, which do not necessarily have directly recognisable physical meaning. The kinematical quantities and the spatial curvature are intuitively comprehended and therefore it is useful to write the Einstein tensor with respect to them.

2.3 Solving the field equations

Above the Einstein field equation and its components G_{ab} and T_{ab} are introduced in detail. Amongst many aspects, it is noted that the Einstein field equation includes 10 linearly independent equations. In addition, the Bianchi identity and the Einstein field equation were found to introduce four additional equations in the system via the conservation of energy-momentum tensor. These equations lay the foundation for the dynamics of any system described by general relativity.

2.3.1 Decomposition of the equations

As the energy-momentum tensor is decomposed into parts parallel and orthogonal to the four-velocity, it is convenient to perform the same 1+3 decomposition for the Einstein field equation as well. In order to do this, let us rewrite the Einstein field equation as

$$ R_{ab} = T_{ab} - \frac{1}{2}T g_{ab} + \Lambda g_{ab}, \tag{2.89} $$

where $T = T^c{}_c$. The 1+3 decomposition of the above expression yields

$$ R_{ab}u^a u^b = \frac{1}{2}(\rho + 3p) - \Lambda, \tag{2.90} $$

$$ R_{ab}u^a h^b{}_c = -q_c, \tag{2.91} $$

$$ R_{ab}h^a{}_c h^b{}_d = \left[\frac{1}{2}(\rho - p) + \Lambda\right] h_{cd} + \pi_{cd}, \tag{2.92} $$

where the energy-momentum tensor (2.56) is assumed. The latter two equations yield dynamical equations for vorticity and shear and some constraining equations, whereas the uppermost equation gives the well-known Raychaudhuri equation.

Let us derive the Raychaudhuri equation by first taking the trace of the Ricci identity (2.32), which results in the Ricci tensor with respect to the four-velocity as

$$(\nabla_a \nabla_d - \nabla_d \nabla_a) u^a = R_{bd} u^b. \tag{2.93}$$

Contracting with u^d gives

$$\nabla_a \dot{u}^a - \nabla_a u^d \nabla_d u^a - \dot{\Theta} = R_{bd} u^b u^d. \tag{2.94}$$

Noting that $\omega_a{}^d \omega_d{}^a = -2\omega^2$, $\sigma_a{}^d \sigma_d{}^a = 2\sigma^2$, $h_a{}^d h_d{}^a \Theta^2/9 = \Theta^2/3$ and the other components of $\nabla_a u^d \nabla_d u^a$ are zero, one finds

$$\nabla_a \dot{u}^a - (2\sigma^2 - 2\omega^2 + \frac{1}{3}\Theta^2) - \dot{\Theta} = R_{bd} u^b u^d. \tag{2.95}$$

Substituting the Einstein field equation (2.89) and the energy-momentum tensor (2.56) in the above equation, the well-known Raychaudhuri equation is obtained:

$$\dot{\Theta} + \frac{1}{3}\Theta^2 - \dot{u}^a{}_{;a} + 2(\sigma^2 - \omega^2) = -\frac{1}{2}(\rho + 3p) + \Lambda. \tag{2.96}$$

It describes the dynamics of the volume expansion Θ, thus being a significant equation in cosmological models.

The 1+3 decomposed Eqs. (2.74), (2.75), (2.90), (2.91), and (2.92) are equivalent to (2.89) (or (2.1)) and (2.73).

2.3.2 Solving the field equations

Simplifications of the Einstein field equation and the conservation of energy-momentum tensor are frequently applied due to the complexity of the equations. A simplification is often considered as an averaging procedure over large, cosmological scales. A rather common approach is to take an averaged metric and substitute it in the equations. This procedure is, however against the common practice in physics, where any system should be averaged as a whole instead of averaging its components. In this case, the

Einstein tensor G_{ab} is dependent on the metric tensor g_{ab} and in general the average of the Einstein tensor $\langle G_{ab}(g_{ab})\rangle$ is not equivalent to the Einstein tensor with respect to the average metric $G_{ab}(\langle g_{ab}\rangle)$, that is

$$\langle G_{ab}(g_{ab})\rangle \neq G_{ab}(\langle g_{ab}\rangle). \tag{2.97}$$

However, $G_{ab}(\langle g_{ab}\rangle)$ can be considered as an approximation of $\langle G_{ab}(g_{ab})\rangle$ and therefore be physically viable.

2.4 Cosmological models

I shall next bring out the averaging problem by presenting Friedmann's and Buchert's approaches to homogeneous and isotropic universes, the former assumes $G_{ab}(\langle g_{ab}\rangle)$ and the latter $\langle G_{ab}(g_{ab})\rangle$. I shall also write the equations for the Lemaître-Tolman-Bondi (LTB) models studied in [1, 2, 4] and for the type IX Bianchi models studied in [3].

2.4.1 Fiedmann's model

In the Friedmann model, the orbits are space-like and three-dimensional ($s = 3$) and the Killing vector fields generate an isotropy group of dimension $d = 3$ at each point of an orbit. That is, the space is homogeneous and isotropic thus complying with the cosmological principle. The metric of such space-time is called the Friedmann-Lemaître-Robertson-Walker (FLRW) metric and it can be written as

$$ds^2 = -dt^2 + a^2\left\{\frac{dr^2}{1-kr^2} + r^2[d\theta^2 + \sin^2(\theta)d\phi^2]\right\}, \tag{2.98}$$

where $a = a(t)$ and $k = +1$, 0, or -1 respectively for hyperbolic, parabolic, or elliptic space. The energy-momentum tensor (2.56) assumes the perfect fluid form ($q^a = 0 = \pi^{ab}$) and the observer is comoving with the fluid flow. Therefore, the four-velocity of the fluid reads as in Eq. (2.59) and the observer experiences no shear, vorticity, or acceleration, that is, $\omega = \sigma = \dot{u} = 0$.

By using Eq. (2.81), the Raychaudhuri Eq. (2.96) assumes the form

$$\dot{H} + H^2 = -\frac{1}{6}(\rho + 3p) + \frac{\Lambda}{3}, \tag{2.99}$$

the conservation of energy-momentum tensor reduces to

$$\dot{\rho} + 3H(\rho + p) = 0, \quad h_a{}^b \nabla_b p = 0, \tag{2.100}$$

and the equation for the spatial curvature (2.88) reads as

$${}^3R = -6H^2 + 2\rho + 2\Lambda. \tag{2.101}$$

The rest of the components of the Einstein field equation are identically zero. Using the definition for Θ one finds $H = \dot{a}/a$ and hence the Hubble parameter depends only on time. Moreover, the latter of Eqs. (2.100) imply that the pressure can depend only on time due to the vanishing spatial pressure gradients. Consequently, ρ and ${}^3R$ depend only on time too (because of Eqs. (2.99) and (2.101)) and therefore the whole dynamical system is dependent only on time.

2.4.2 Buchert's model

In Ref. [21] was demonstrated that tensors can lose their invariance under coordinate transformations after the averaging. This implies that scalars are the only tensors with well-defined averages as scalar equations remain invariant under coordinate transformation. In Buchert's approach, first formulated in [22], this was acknowledged by averaging only scalar quantities.

In Ref. [22], the matter source is irrotational ($\omega = 0$) dust and the coordinates are chosen to be comoving with the fluid ($u^a = \delta^a_0$). The line-element can now be chosen to be of the form (2.55). The Einstein field equation, conservation of energy-momentum tensor and Eq. (2.88) yield three scalar equations: the Raychaudhuri equation

$$\dot{\Theta} = -2\sigma^2 - \frac{1}{3}\Theta^2 - \frac{1}{2}\rho + \Lambda, \tag{2.102}$$

the energy conservation equation

$$\dot{\rho} = -\Theta\rho, \tag{2.103}$$

and the Hamiltonian constraint

$${}^3R = -\frac{2}{3}\Theta^2 + 2\rho + 2\sigma^2 + 2\Lambda, \tag{2.104}$$

where the dot denotes derivation with respect to time. These three equations corresponds to Eqs. (2.99), (2.100), and (2.101) of the Friedmann model, however with a few important differences. The Friedmann model includes pressure, which is absent here, whereas the shear is zero in the Friedmann model but not here. Excluding the shear and pressure, Eqs. (2.99), (2.100), and (2.101) formally appear similar as Eqs. (2.102), (2.103), and (2.104), but have a distinct difference: the Friedmann equations depend only on time, whereas the Buchert equations depend also on location.

In order to obtain the location independent equations of motion, Ref. [22] continue by introducing an averaging procedure. To assure the coordinate invariance, Buchert defines the spatial average of a scalar field $S(t, x^i)$ as

$$\left\langle S(t,x^i)\right\rangle_{\mathcal{D}} \equiv \frac{\int_{\mathcal{D}} S(t,x^i)\sqrt{\hat{h}}dx^3}{\int_{\mathcal{D}}\sqrt{\hat{h}}dx^3}, \tag{2.105}$$

where $\hat{h} = det[\hat{h}_{ij}(t,x^i)]$, and $\mathcal{D}$ is an averaging domain, which is a compact portion of a constant time hypersurface. The volume of a spatial hypersurface inside a domain $\mathcal{D}$ is

$$V_{\mathcal{D}}(t) = \int_{\mathcal{D}}\sqrt{\hat{h}}dx^3. \tag{2.106}$$

This enables introducing a dimensionless time-dependent scale factor that is effective inside a spatial domain $\mathcal{D}$,

$$a_{\mathcal{D}}(t) \equiv \left(\frac{V_{\mathcal{D}}(t)}{V_{\mathcal{D}}(t_0)}\right)^{1/3}, \tag{2.107}$$

where t_0 denotes present time. The average expansion rate within $\mathcal{D}$ can be now given,

$$\langle\Theta\rangle_{\mathcal{D}} = \frac{\int_{\mathcal{D}}\partial_t\sqrt{\hat{h}}dx^3}{\int_{\mathcal{D}}\sqrt{\hat{h}}dx^3} = 3\frac{\dot{a}_{\mathcal{D}}}{a_{\mathcal{D}}}, \tag{2.108}$$

giving also rise to the domain dependent Hubble function,

$$\mathcal{H}_{\mathcal{D}} \equiv \frac{1}{3}\langle\Theta\rangle_{\mathcal{D}}\,. \tag{2.109}$$

Taking the average of both sides of Eqs. (2.102) and (2.103) yields the components $\langle\dot{\theta}\rangle_{\mathcal{D}}$ and $\langle\dot{\rho}\rangle_{\mathcal{D}}$. In order to obtain proper differential equations, these components need to be expressed in terms of $\langle\theta\rangle_{\mathcal{D}}$, $\langle\sigma\rangle_{\mathcal{D}}$, $\langle\rho\rangle_{\mathcal{D}}$, and $\langle{}^3R\rangle_{\mathcal{D}}$ or their time derivatives. By applying Eqs. (2.105), (2.108) and noting that

$$\Theta = \nabla_\mu u^\mu = \Gamma^\mu_{\mu 0} = \frac{\partial_t\sqrt{\hat{h}}}{\sqrt{\hat{h}}} = \hat{h}^{ij}\partial_t\hat{h}_{ij}, \tag{2.110}$$

the time derivative of any spatially averaged quantity can be written as

$$\partial_t \langle S\rangle_{\mathcal{D}} = \langle\partial_t S\rangle_{\mathcal{D}} + \langle\Theta S\rangle_{\mathcal{D}} - \langle S\rangle_{\mathcal{D}}\langle\Theta\rangle_{\mathcal{D}}\,. \tag{2.111}$$

By defining the so-called backreaction,

$$\mathcal{Q}_{\mathcal{D}}(t) \equiv \frac{2}{3}\left(\left\langle\Theta^2\right\rangle_{\mathcal{D}} - \langle\Theta\rangle^2_{\mathcal{D}}\right) - 2\left\langle\sigma^2\right\rangle_{\mathcal{D}}, \tag{2.112}$$

the averaged scalar equations (2.104), (2.102) and (2.103) can be written as

$$3\frac{\ddot{a}_{\mathcal{D}}(t)}{a_{\mathcal{D}}(t)} = -\frac{\kappa}{2}\langle\rho\rangle_{\mathcal{D}}(t) + \mathcal{Q}_{\mathcal{D}}(t) + \Lambda \tag{2.113}$$

$$3\left(\frac{\dot{a}_{\mathcal{D}}(t)}{a_{\mathcal{D}}(t)}\right)^2 = \kappa\langle\rho\rangle_{\mathcal{D}}(t) - \frac{1}{2}\left\langle{}^{(3)}R\right\rangle_{\mathcal{D}}(t) - \frac{1}{2}\mathcal{Q}_{\mathcal{D}}(t) + \Lambda \tag{2.114}$$

$$\partial_t\langle\rho\rangle_{\mathcal{D}}(t) = -3\frac{\dot{a}_{\mathcal{D}}(t)}{a_{\mathcal{D}}(t)}\langle\rho\rangle_{\mathcal{D}}(t) \tag{2.115}$$

These equations are recognised as the Buchert equations, and differ from the Friedmann equations in two ways; Buchert equations are domain dependent and contain the backreaction function. These equations have been generalised in Ref. [23].

2.4.3 Lemaitre-Tolman-Bondi models

The line-element containing two-dimensional space-like orbits clearly includes the special case

$$ds^2 = -dt^2 + \tilde{R}^2 dr^2 + R^2\left(d\theta^2 + \sin^2\theta\, d\phi^2\right), \tag{2.116}$$

which is radially inhomogeneous but spherically symmetric with respect to one point ($\tilde{R} = \tilde{R}(r,t)$ and $R = R(r,t)$). By assuming a model which obeys such metric, has $\Lambda = 0$, and is sourced only by dust (which is comoving with a frame orthogonal to the surfaces of homogeneity), one obtains the LTB model first studied by Lemaître [24] and Tolman [25] and later by Bondi [26].

Applying the metric Eq. (2.116) to the Einstein field equation (2.1) yields four algebraically independent equations. Three of these equations are functionally independent and after some manipulation can be presented as

$$\tilde{R} = \frac{R_{,r}}{\sqrt{1+2e(r)^2}}, \tag{2.117}$$

$$\left(\frac{R_{,t}}{R}\right)^2 = \frac{2M(r)}{R^3} + \frac{2e(r)r^2}{R^2} + \frac{\Lambda}{3}, \tag{2.118}$$

$$\rho = 2\frac{M_{,r}(r)}{R_{,r}R^2}, \tag{2.119}$$

where $M(r)$ and $e(r)$ are undetermined functions emerging from integration over t, but $e(r)$ is constrained by $2e(r)r^2 \geq -1$. A parameter after a comma means partial derivation with respect to the parameter.

The fluid in the LTB models is pressure-less perfect fluid. Therefore, the momentum part of the conservation of energy-momentum tensor, Eq. (2.75), vanishes identically, whereas Eq. (2.119) is a solution for the equation rising from the energy part of the conservation of energy-momentum tensor, Eq. (2.74).

2.4.4 Axisymmetric Bianchi IX model

Here is presented the axisymmetric type IX Bianchi model studied in Ref. [3]. The used line-element was obtained from Ref. [27]:

$$ds^2 = -dt^2 + e^{2\alpha+2\beta}\left[(\omega^1)^2 + (\omega^2)^2\right] + e^{2\alpha-4\beta}(\omega^3)^2\,, \tag{2.120}$$

where the one-forms ω^i read as

$$\omega^1 = \sin\psi d\theta - \sin\theta\cos\psi d\phi\,, \tag{2.121}$$
$$\omega^2 = \cos\psi d\theta + \sin\theta\sin\psi d\phi\,, \tag{2.122}$$
$$\omega^3 = \cos\theta d\phi + d\psi\,. \tag{2.123}$$

As the homogeneous space-like orbits are three dimensional, the dynamical functions are only dependent on time: $\alpha = \alpha(t)$ and $\beta = \beta(t)$.

The energy-momentum tensor is of the form (2.56) with $\pi_{ab} = 0$ and the four-velocity is chosen to be as in Eq. (2.62), hence the fluid is tilted with respect to the coordinate system. The fluid is assumed to obey the equation of state (2.67) with the time-dependent equation of state parameter, $w = w(t)$. The Einstein field equation does not yield a dynamical equation for $w(t)$, hence it is to be determined by using additional assumptions. The cosmological constant is assumed to vanish.

In Ref. [3] we employ the standard notation for the expansion normalised quantities

$$\Omega = \frac{\rho(t)}{3H^2}, \quad K = -\frac{{}^3R(t)}{6H^2}, \tag{2.124}$$

but in order to shorten the presentation of the dynamical equations, a novel notation for the Hubble parameter and for the expansion normalised shear and vorticity is introduced:

$$H \equiv \frac{\Theta(t)}{3\cosh[\lambda(t)]}, \quad \Sigma \equiv \frac{\sigma(t)}{\sqrt{3}\cosh[\lambda(t)]H}, \quad \mathcal{V} \equiv \frac{\omega(t)}{\sinh[\lambda(t)]H}. \tag{2.125}$$

During the time interval where $0 < \alpha'(t)$, α can be used as conformal time. The volume expansion is related to α as $H = \alpha'(t)$, therefore, for any function $f(t)$,

$$\frac{f'(t)}{H(t)} = \frac{f'(t)}{\alpha'(t)} = f'(\alpha)\,, \tag{2.126}$$

where the prime denotes differentiation with respect to the argument. Applying this to the conservation of energy-momentum tensor and the Einstein field equation yield four dynamical equations,

$$\Sigma'(\alpha) = -1 + 2K(\alpha) + \Sigma(\alpha)^2 + (\epsilon - 3)\Sigma(\alpha) + \mathcal{V}(\alpha)^2 + \Omega(\alpha)\,, \tag{2.127}$$

$$\begin{aligned}\Omega'(\alpha) &= \Omega(\alpha)\left(2\epsilon + 2\Sigma(\alpha) - 4 + \frac{1-3w-2\Sigma(\alpha)}{W(\alpha)}\right) \\ &\quad -\frac{\Omega(\alpha)}{W(\alpha)}W'(\alpha)\,, \end{aligned} \tag{2.128}$$

$$\mathcal{V}'(\alpha) = \mathcal{V}(\alpha)\left(\epsilon - 4\Sigma(\alpha) - 1\right)\,, \tag{2.129}$$

$$K'(\alpha) = -2\left\{K(\alpha)[-\epsilon + 1 + \Sigma(\alpha)] + \Sigma(\alpha)\mathcal{V}(\alpha)^2\right\}\,, \tag{2.130}$$

and one constraining equation,

$$1 = W(\alpha)\Omega(\alpha) + K(\alpha) + \Sigma(\alpha)^2\,, \tag{2.131}$$

where the auxiliary functions

$$\epsilon = \frac{1}{2}\left[3w(\alpha) - 1\right]\Omega(\alpha) - K(\alpha) + 2 + \Sigma(\alpha)^2\,, \tag{2.132}$$

$$W(\alpha) \equiv \frac{1}{2}\left(1 - w(\alpha) + \frac{w(\alpha)+1}{\cosh[2\lambda(\alpha)]}\right)\,, \tag{2.133}$$

have been exploited. Let us note that $\epsilon \equiv -H'(t)/H(t)^2$ and that the momentum Eq. (2.75) vanishes here identically.

Chapter 3

Standard cosmology

The cosmological principle is one of the cornerstones of the cosmological standard model, but there is much more involved. In this chapter, I shall briefly introduce the standard cosmological model by the parts relevant to the rest of the book. In particular, I shall discuss its acceleration history and present some of its observational success. The framework of the cosmological standard model is well established, but all the details are not written in stone. The short review below gives one version.

3.1 ΛCDM model

The cosmological standard model, the Λ cold dark matter (ΛCDM) model, is capable of darning different eras and phenomena together in concordance with each other and most of the cosmological observations. The evolution of the background geometry of the universe is described using the FLRW metric (2.98) throughout the history. That is, the evolution of the background geometry is similar everywhere and in every direction and therefore determined by the evolution of a single scale factor $a(t)$, which is the only variable in the line-element (2.98). The dynamics of the scale factor is dictated by Eq. (2.101) and the energy content of the universe. By introducing the dimensionless and expansion normalised quantities

$$\Omega = \frac{\rho}{3H^2}, \quad K = -\frac{{}^3R}{6H^2}, \quad \Omega_\Lambda = \frac{\Lambda}{3H}, \tag{3.1}$$

and substituting them in Eq. (2.101) yields

$$1 = \Omega + K + \Omega_\Lambda. \tag{3.2}$$

This equation constraints quantities (3.1) so that simply comparing their values reveals which type of energy density is dominating the energy budget of the universe at a given time. Taking into account that dust, radiation, and curvature dilutes respectively as $\propto a^{-3}$, $\propto a^{-4}$, and $\propto a^{-2}$, one can rewrite Eq. (3.2) as

$$H^2 = H_0^2 \left[\Omega_{m_0} \left(\frac{a_0}{a} \right)^3 + \Omega_{r_0} \left(\frac{a_0}{a} \right)^4 + \Omega_{k_0} \left(\frac{a_0}{a} \right)^2 + \Omega_\Lambda \right], \tag{3.3}$$

where decomposition (2.72) have been employed and $H_0 = H(t_0)$, $\Omega_{m_0} = \Omega_m(t_0)$, $\Omega_{r_0} = \Omega_r(t_0)$, $\Omega_{k_0} = \Omega_k(t_0)$, $a_0 = a(t_0)$ with t_0 being the present time. Eq. (3.3) is known as the Friedmann equation.

The expansion history of the universe is characterised by the assumption that the universe has expanded since its beginning. The phenomena taking place during the first moments are under speculation (and what does the first moments even mean) but it is assumed that fairly quickly the universe becomes sufficiently homogeneous and isotropic; the era reckoned to be responsible for this is called inflation. The hypothesis that inflation makes the universe homogeneous and isotropic relies on the cosmic no-hair conjecture. It is based on a theorem which states that the eternally expanding homogeneous cosmological models approach the de Sitter solution, if the models satisfy the Einstein field equation with $0 < \Lambda$ and the energy-momentum tensor comply with the dominant and strong energy conditions [28].[1] The likelihood for an inflation to emerge from generic initial conditions is still under a debate as different inflationary scenarios and evaluation methods yield inconsistent results [29]. Observations have not been able to specify the preferred inflationary scenario, but a rather common assumption is that it is driven by a scalar field (or fields) called the inflaton. In such scenarios, a rather commonly accepted feature is that the inflation has to last $\gtrsim 50$ e-folds, that is the scale factor has to be $\gtrsim 50$ e-folds larger at the end of the inflation than it was at the beginning. However, the expected number of e-folds of a given inflationary scenario can be much higher that 50 [30].

Inflation is followed by an era where the inflaton field decays into particles due to various complex procedures, like non-perturbative and perturbative decay [31]. The details of this era, often dubbed as reheating, are

[1] An additional condition is required for the theorem to hold for the type IX Bianchi models: the cosmological constant needs to be large enough compared with the spatial curvature.

not completely understood for several reasons. One of them is the uncertainty in the inflationary scenario as different scenarios result in different decay mechanisms. Another aspect blurring the details of reheating is the non-linearity of the governing equations which makes the decay procedure complex and hard to follow analytically. Nonetheless, the majority of the reheating models result in a radiation dominated universe that has reached local thermal equilibrium. Hence, the universe has transfered to a radiation dominated era. As radiation dilutes faster in an expanding universe than dust, the universe gradually becomes dominated by dust. Photons decouple from matter shortly after the radiation-matter equality, this era is known as decoupling. The only component in our universe that does not dilute as the universe expands is Λ and hence, after time has passed sufficiently, the universe undergoes a transition from matter to cosmological constant domination; the universe has recently gone through this transition.

Most of the cosmological observations are in agreement with the flat ΛCDM model [32, 33] and the latest Planck data reports the best fit values $\Omega_m = 0.3089 \pm 0.0062$ and $H_0 = 67.74 \pm 0.46$ [33] for combined Planck, supernova Ia, H_0, and baryon acoustic oscillation data sets. However, some observations are in tension with the ΛCDM model and these issues are discussed in the following chapter.

3.2 Observations

3.2.1 Supernovae

Accretion of a white dwarf over the Chandrasekhar limit (about 1.4 Solar masses) is expected to initiate a thermonuclear explosion. This process is expected to result in the so-called type Ia supernova (SNIa). Even though we cannot take pleasure in fully understanding the process, SNIa is believed to exhibit observationally distinct features which can be used to give an estimate for the distance of a given supernova explosion [34].

The data releases of SNIa surveys include the distance modulus μ and the redshift z for each SNIa event. In FLRW space-times, the redshift is related to the scale factor as

$$\frac{a}{a_0} = \frac{1}{1+z}, \tag{3.4}$$

and the distance modulus is related to the luminosity distance D_L through

the relation

$$\mu = 5 \log_{10} D_L + 25. \tag{3.5}$$

The luminosity distance is related to the angular diameter distance D_A through the equation $D_L = (1+z)^2 D_A$ [35] and $D_A = ar$ for the homogeneous and isotropic metric (2.98). In addition, the metric gives the coordinate distance for a radially propagating light ray by setting $ds = d\theta = d\phi = 0$:

$$\frac{dr}{\sqrt{1-kr^2}} = \pm \frac{dt}{a}, \tag{3.6}$$

where the minus sign corresponds to incoming light. By integration and with the aid of Eq. (3.4), we find:

$$r = \begin{cases} \frac{1}{H_0\sqrt{|\Omega_k|}} \sin\left(\int_0^z \frac{H_0\sqrt{|\Omega_k|}}{H(\tilde{z})} d\tilde{z}\right) & \text{if } k > 0, \\ \int_0^z \frac{1}{H(\tilde{z})} d\tilde{z} & \text{if } k = 0, \\ \frac{1}{H_0\sqrt{|\Omega_k|}} \sinh\left(\int_0^z \frac{H_0\sqrt{|\Omega_k|}}{H(\tilde{z})} d\tilde{z}\right) & \text{if } k < 0. \end{cases} \tag{3.7}$$

Now the distance modulus μ can be given with respect to z within the framework of the Friedmann models. Consequently, the preferred values for the free parameters of the model can be obtained from (μ, z) data using statistical methods. The authors of Refs. [36, 37] were the first to notice that the SNIa distance estimators favoured the existence of a positive cosmological constant. The sequential analyses have confirmed these results and the most recent analysis for a flat ΛCDM model gives $\Omega_m = 0.295 \pm 0.034$ [38].

3.2.2 Local Hubble value

As described in Sec. 3.2.1, the luminosity distance can be expressed with respect to the redshift, $D_L = (1+z)a(z)r(z)$. For the close by objects having redshifts smaller than unity, $D_L(z)$ can be expanded in a Taylor series, giving

$$D_L = \frac{1}{H_0}\left(z - \frac{1}{2}(1-q_0)z^2\right) + \mathcal{O}(z^3), \tag{3.8}$$

where H_0 is the local Hubble value, $q_0 \equiv -\ddot{a}_0 a_0/\dot{a}_0^2$ is the so-called deceleration parameter. Note that Eq. (3.8) is independent on the curvature parameter k. Assuming q_0 is obtained from other observations, the best fit local Hubble value can be evaluated from a set of (μ, z) data (or from (D_L, z) data, see Eq. (3.5)).

The local Hubble value was determined using Cepheid variables in Ref. [39]. The (μ, z) data of the Cepheids host galaxies was known via SNIa observations and the deceleration parameter was fixed[2] $q_0 = -0.55$; they found the best fit value $H_0 = 73.8 \pm 2.4$ km s^{-1} Mpc^{-1}. They were able to improve the accuracy of their results due to the observations of Cepheids in new host galaxies with known (μ, z) relation. The new best fit turned out to be $H_0 = 73.02 \pm 1.79$ km s^{-1} Mpc^{-1} [40]. On the other hand, Ref. [41] reanalysed the data and found $H_0 = 70.6 \pm 3.3$ km s^{-1} Mpc^{-1}. Hence, it appears that the process for locally evaluating H_0 is not fully comprehended.

3.2.3 Baryon acoustic oscillations

Baryon acoustic oscillation (BAO) surveys track spherical wavefronts in the galaxy distribution. According to the ΛCDM model, these wave fronts are remnants of the pressure waves from the era where matter and radiation were coupled. Roughly speaking, after the radiation and matter stopped interacting, at the decoupling time, the pressure waves froze and since have been affected only by gravity [42].

Using Eq. (3.4) and the metric (2.98) the diameter of a spherical wavefront in the radial direction can be given as

$$\Delta z_{BAO} = (1+z)H(z)l_{phys} = H(z)l^c_{phys}, \tag{3.9}$$

where l_{phys} is the physical length of the radius of the spherical wavefront ($l_{phys} \approx ds$) and $l^c_{phys} = (1+z)l_{phys}$ is its comoving counterpart. In the ΛCDM model the physical length is obtained from the speed of the sound waves at the decoupling time. The corresponding equation for the angular diameter is given explicitly in the metric (2.98),

$$\Delta\theta_{BAO} = \frac{l_{phys}}{D_A} = \frac{l^c_{phys}}{D^c_A}, \tag{3.10}$$

[2]This value for q_0 is consistent with the ΛCDM model with $\Omega_k = 0$ and $\Omega_m = 0.3$.

where $D_A^c = (1+z)D_A$ is the comoving angular distance. Furthermore, the two diameters can be combined to give a measure for the volume of the sphere:

$$d_{z_{BAO}} = \left(\Delta\theta_{BAO}^2 \frac{\Delta z_{BAO}}{z_{BAO}}\right)^{1/3}. \tag{3.11}$$

The BAO surveys report their results in $d_{z_{BAO}}$, $\Delta\theta_{BAO}$, or Δz_{BAO} with respect to the effective redshift z_{eff}. Low redshift ($z_{eff} < 1$) BAO results by 6dF Galaxy Survey (6dFGS) [43] at $z_{eff} = 0.106$, Sloan Digital Sky Survey (SDSS) [44, 45] at $z_{eff} = 0.35$ and $z_{eff} = 0.57$, and WiggleZ survey [46] at $z_{eff} = 0.44$, $z_{eff} = 0.60$ and $z_{eff} = 0.73$ are compatible with the nine-year WMAP data [47]. The results by 6dFGS, more up to date analyses of SDSS by [48] at $z_{eff} = 0.15$ and [49] at $z_{eff} = 0.32$ and $z_{eff} = 0.57$ are compatible with the latest Planck data, yielding $H_0 = 67.6 \pm 0.6$ km s^{-1} Mpc^{-1} and $\Omega_m = 0.310 \pm 0.008$ for a flat ΛCDM model[33]. [3]

3.2.4 Cosmic microwave background radiation

In modern cosmology, the assumption that the universe has expanded to the present state from a denser state is nearly a model independent. In such models, it is inevitable for the photons to decouple from dust at some point and propagate practically without scattering thereafter. Such epoch is referred to as decoupling epoch and it effectively defines a surface where photons scatter the last time, the surface of last scattering. We observe ~ 3 K radiation in each direction in the sky and assume it originates from the surface of last scattering; this radiation is called the cosmic microwave background (CMB) radiation. Because the radiation has the same temperature in each direction, it is justified to approximate (in temperature-wise) that the surface of last scattering is a sphere and we are in the centre of it. Therefore, the surface of last scattering can be modelled with spherical harmonics $Y_{lm}(\theta, \phi)$ by doing a multipole expansion for the temperature contrast:

$$\frac{\delta T}{T}(\theta, \phi) = \sum_{l,m} a_{lm} Y_{lm}(\theta, \phi). \tag{3.12}$$

[3] The WiggleZ data is excluded from the analysis of Ref. [33] due to the unquantified correlation between WiggleZ and [49] at $z_{eff} = 0.57$.

Here, T is the average temperature at the last scattering surface and δT is a small deviation from T. The sum runs over $l = 1, 2, \ldots, \infty$ and $m = -l, -l+1, \ldots, l-1, l$. The spherical harmonics are orthogonal to each other and the multipole coefficients are obtained from

$$a_{lm} = \int Y^*_{lm}(\theta, \phi) \frac{\delta T}{T}(\theta, \phi) d\Omega. \tag{3.13}$$

Dipole, quadrupole, and octopole correspond to l values 1, 2, and 3, respectively. In cosmological context, the dipole has a special role because it is difficult to evaluate how much of it is due to cosmic origin and how much due to our peculiar velocity with respect to the CMB frame. Therefore, the dipole is usually examined separately from the other multipoles and it is a common practice that multipoles having $l < 2$ are excluded when discussing low multipoles (or large angles). I shall also use this common convention. The two point correlation function is

$$W(\theta) \equiv \frac{\langle \delta T(\gamma) \delta T(\gamma') \rangle}{T^2}, \tag{3.14}$$

where γ and γ' are unit vectors, $\gamma \cdot \gamma' = \cos\theta$, and the average is taken over all pairs of points separated by angle θ in the CMB sky.

In the standard description, the factors a_{lm} are taken to be Gaussian random variables and independent on m. Furthermore, as a_{lm} describe a deviation from the average temperature, they have zero expectation value ($\langle a_{lm} \rangle = 0$), and it is convenient to introduce the so-called theoretical angular power spectrum

$$C_l \equiv \langle |a_{lm}|^2 \rangle = \frac{1}{2l+1} \sum_m \langle |a_{lm}|^2 \rangle. \tag{3.15}$$

The theoretical angular power spectrum represents our expectation of the CMB of all the possibilities whereas we observe only one realisation of which angular power spectrum $\hat{C}_l$ is defined as

$$\hat{C}_l \equiv \frac{1}{2l+1} \sum_m |a_{lm}|^2. \tag{3.16}$$

The variance of $\hat{C}_l$,

$$\langle(\hat{C}_l - C_l)^2\rangle = \frac{2}{2l+1}C_l^2, \tag{3.17}$$

is called the cosmic variance and gives the limits for the accuracy of our measurements that cannot be exceeded by any means.

The information about the temperature fluctuations is in C_l via Eqs. (3.13) and (3.15) and the assumptions of the standard cosmology enable extracting information from C_l. For example, taking the flat six-parameter ΛCDM model to represent standard cosmology, six parameter values can be extracted from the CMB. Here, only two parameters, Ω_m and H_0, are needed and they are derived from these six fit parameters. For the flat six-parameter ΛCDM model, the nine-year CMB data by WMAP gives the best fit values for the baryon density $\Omega_b = 0.0463 \pm 0.0024$, cold dark matter density $\Omega_c = 0.233 \pm 0.023$ ($\Omega_m = \Omega_c + \Omega_b$), and $H_0 = 70.0 \pm 2.2$ [47]. The latest Planck data [33] gives the best fit values $\Omega_m = 0.308 \pm 0.012$ and $H_0 = 67.8 \pm 0.9$ for the same model.

Chapter 4

Cosmology beyond the cosmological principle

The universe is inhomogeneous and anisotropic, at least in small scales. Such theoretical models do exists and they have been studied, however, they are very cumbersome. It is beneficial to study simpler models first, like those exhibiting only inhomogeneity or anisotropy, before proceeding to more general models. After learning the benefits and the drawbacks of such simpler models, we are more instructed to investigate the more general and cumbersome inhomogeneous and anisotropic models.

In this chapter, I shall review some of the problems of the ΛCDM model and present attempts to solve these problems by employing models that go beyond the cosmological principle.[1] I will mostly concentrate on the LTB and the Bianchi models, but also discuss more general models. This gives perspective on the comprehension how simpler models have affected the investigation of more cumbersome models. As the cosmological principle refers to space-time, the Buchert formalism can be acknowledged to go beyond the principle, albeit it is statistically homogeneous and isotropic. I shall shortly discuss Buchert's formalism, too.

4.1 Apparent acceleration

The concordance cosmological ΛCDM model assumes the existence of the mystical constant Λ. The mystique of Λ probably originates from the idea that Λ should arise from quantum field theory and embody the vacuum

[1] The list of incompatibilities I shall present below is not comprehensive and further discrepancies between the ΛCDM model and observations are listed e.g. in [50, 33].

energy density in cosmic scales. Quantum field theory, as it is currently understood, predicts a finite number for the quantised vacuum energy density by imposing a cut-off scale. However, if the cut-off is at the Planck scale, as is usually assumed, quantum field theory predicts Λ to be some 120 orders of magnitude larger than cosmological observations indicate [51, 52]. This is known as the old cosmological constant problem. This problem was acknowledged well before the SNIa observations [36, 37], which invoke the new cosmological constant problem: why is $\Omega_\Lambda \sim 1$ today? The significance of these problems is debatable and Λ does not need to be mystical if one simply assumes it is a constant of nature, like Newton's gravitational constant [53]. Whatever the truth, the hypothesis of Λ is to be tested. Consequently, the cosmological constant problems have extended to the so-called dark energy problem, which suggests Λ is not responsible for accelerating the universe but some other effect is instead. Probably the most popular approaches to the dark energy problem are the dark energy and the modified gravity models [51, 52], but present observations are not accurate enough to distinguish between them and the ΛCDM model [54]; future observations are expected to clarify this issue [42].

The cosmological constant, dark energy, and modified gravity all imply that accelerating expansion is required in order to explain the SNIa data. The same data, however, can result from differential expansion with respect to location so that no region is accelerating. This requires inhomogeneity and suggests acceleration is only required in the FLRW space-times, that is, the acceleration is apparent.

4.1.1 Inhomogeneity

As mentioned above, by discarding the assumption of the FLRW space-time and exploring more general solutions of the Einstein field equation and conservation of energy and momentum, the dimming of supernovae can be explained using radially inhomogeneous LTB models without dark energy, modified gravity or Λ. This was first proposed in Ref. [55], where also an example was given. Since then, it has been shown that the LTB and ΛCDM models provide a comparable fitting for SNIa data [56, 57, 58, 59, 60, 61, 62]. These promising results induced further interest towards the models. Because the LTB models are inhomogeneous only radially and the inhomogeneity explaining the SNIa is typically notable, the interest have focused on two aspects: the fine-tuning of the observer's location and other

cosmological observations.

Fine-tuning of the observer's location

As the LTB models admit a preferred point in space, the centre of spherical symmetry, it was presumed that the isotropy of the observations would place Earth in the vicinity of the preferred point. In [63] was studied how far the observers can be removed from the symmetry centre without discrepancy to SNIa and CMB dipole data. They found that the observer should not be located further away than $\sim 1\%$ of the radius of the void or the dipole amplitude becomes too large (order of 10^{-3} is the maximum for the amplitude). Another approach to this issue was conducted by the authors of Ref. [58]. First they found that SNIa data constrains the observer in the vicinity of the centre within $\sim 15\%$ of the radius of the void. Including the CMB dipole data this number dropped to $\sim 1\%$. They also studied how extra velocity of the observer would affect here. Larger velocity allows for larger displacement, but larger displacement away from the centre induces deterioration of the fit of SNIa data.

An interesting question is whether the fine-tuning issue vanishes in more complex models than the spherically symmetric LTB model, suitable candidates for studying this are e.g. the Szekeres models. Indeed, it has been shown that these models permit Earth to be further shifted from the centre of the void than the LTB models [64]. However, it appears that the fine-tuning issue only emerges elsewhere and does not disappear: in the quasispherical models, the observer's location is fine-tuned close to a point where the shear disappears (which is not at the symmetry centre) [65].

Of course, it could be that the fine-tuning issue vanishes when fully general Szekeres, or even more general models are considered. Fully general Szekeres models do not admit any Killing vector fields but are special as the magnetic part of the Weyl tensor (2.43), the vorticity and the fluid acceleration is zero [19]. More general models can be constructed e.g. by "gluing" LTB or Szekeres models together, see e.g. Refs. [66, 67].

Nevertheless, it is not know whether the fine-tuning issue simply disappears by employing more general models. We confront the fine-tuning issue by employing a different approach in papers [1, 4]. The approach will be further discussed in Chapter 5

Cosmological observations

The LTB models contain only dust, hence they hardly serve as a fair approximation throughout the history of the universe. This is problematic as the universe is expected to undergo a radiation dominated period before the matter domination. Consequently, only the local observations can reliably be fitted, like SNIa, local Hubble, and BAO using the LTB model, whereas non-local observations, like CMB, do not enjoy the same pleasure. The approximation is sufficient only, if inhomogeneities become important during matter domination and the evolution before that is described using a model that acknowledges the presence of pressure. The type of scenarios, where a LTB model coincides with the Friedmannian cosmology before radiation becomes important have been ruled out by several authors [60, 61, 68, 69]. We deepened the comprehension for the reason of the failure of these models in [2], this will be discussed in Chapter 5. In these models, however, a significant degree of freedom, the bang time function $t_b(r)$, is constrained to be constant. Such models are called void models. Indeed, SNIa data can be explained using inhomogeneous bang time function alone [70] and fit to other observations improve by removing the constant bang time condition [71, 72]. However, even inhomogeneous $t_b(r)$ is not enough to explain the kinematic Sunyaev-Zel'dovich (kSZ) effect, at least if the effects of radiation are neglected (which I already noted to be quite harsh approximation) [72].

A detailed examination of the above presented studies reveals two matters. First, the LTB models have not been ruled out by covering the effects of pressure sufficiently. Secondly, some of the observables prefer considerable inhomogeneity, like SNIa and combined local Hubble and CMB data, whereas some prefer approximate homogeneity, like the kSZ effect. This discrepancy was further studied in [4], where we investigated whether the LTB models can be "homogenised" while remaining compatible with SNIa data. In fact, we generalised our investigations from the LTB models to the ΛLTB models. Next the ΛLTB models will be introduced.

4.1.2 Inhomogeneity + Λ

It is straightforward to generalise the LTB model to include Λ, the resulting models are called the ΛLTB models. These models introduce interesting possibilities as both the LTB and ΛCDM models are included in the ΛLTB models. The authors of Ref. [73] aimed to discover the best fit ΛLTB model.

However, some of their priors are biased towards the ΛCDM and LTB models, hence it is not surprising that they find observables to prefer these models. In Ref. [61] the authors compared the LTB and ΛCDM models between each other and moreover, tested the Copernican principle. They used only data independent on the details of structure formation, because the linear perturbation theory of the LTB models is poorly understood. Hence, the authors used the Local Hubble rate, SNIa and CMB (but did not include the effects of radiation) observations and assumed the early universe to be homogeneous. They improved the priors used in Ref. [73] e.g. by modelling the local matter density profile by linear interpolation, cubic interpolation and Laguerre polynomials; results were qualitatively similar in each case: reasonable fit to CMB dictates too low H_0, which in their studies can never exceed $H_0 \sim 62$km/s/Mpc and data favours the ΛCDM model. The main result in their studies on the ΛLTB models is interesting. The best fitting model is nearly homogeneous and information criteria[2] favour the ΛCDM model. However, the inhomogeneities can not be ruled out, but $\sim 15\%$ deviations from homogeneity are compatible with the data.

In addition to the ΛLTB models, other approaches to test the robustness of the ΛCDM model against inhomogeneity have also been conducted. The effects of large scale isotropic inhomogeneities to the value of the equation of state parameter w was investigated in Ref. [77]. The best fit value for w is often negative in dark energy models, see e.g. [33], which corresponds to phantom energy that introduces unphysical phenomena. In Ref. [77] was found that the best fit w value corresponding to phantom energy might be due to large scale isotropic inhomogeneities while the true value of w is negative unity. In addition, the filamented large scale structure may alter our estimate for the distance of the surface of last scattering compared with the distance evaluated using the ΛCDM model due to the effects unobtainable using the homogeneous models. When incorporating a modified distance estimate (obtained e.g. from the Dyer-Roeder approximation or from a Swiss-Cheese model) in the ΛCDM model, these effects alter the best fit parameters; in Ref. [78] is demonstrated how C_l becomes modified and for simple toy models the preferred cosmology becomes open with $\Omega_\Lambda \sim 0.8 - 0.9$.

[2]Information criteria takes both likelihoods and the number of free parameters into account. Further information about different information criteria can be found in Refs. [74, 75, 76].

4.1.3 Backreaction

Even though the Buchert equations include Λ, it appears from the mathematical point of view that the backreaction can explain the apparent acceleration and consequently remove the need for Λ. This can be seen from Eqs. (2.102), (2.112), and (2.113): the local expansion θ is decelerating everywhere if $\Lambda = 0$, but the average acceleration $\ddot{a}_{\mathcal{D}}$ in the domain $\mathcal{D}$ is positive as long as the variance of θ is large enough compared with the shear and the fluid density.

Even though mathematically sound, it is not physically evident that Λ can be replaced by a physically viable backreaction. In Ref. [79] is shown how a domain $\mathcal{D}$ causing a backreaction can be composed from an over dense region next to an under dense region: both regions are initially expanding, the over dense region turns eventually to collapse implying large variance for θ in the domain $\mathcal{D}$ and resulting an accelerating $a_{\mathcal{D}}$. This idea is further developed: in Ref. [79], the author illustrates how structure formation can induce average acceleration and moreover, semirealistic models following Ref. [79] have been constructed and the results appear encouraging [80]. However, the effects of a realistic backreaction are still under a debate [81, 82]. These examples illustrate how Buchert's formalism can be used to give an alternative to Λ or dark energy, but the averaging procedure has an impact on other cosmological phenomena too, like light propagation [80].

4.2 Observations

4.2.1 Local Hubble value

Ref. [83] investigates the anisotropy and inhomogeneity of the Hubble flow. They take the COMPOSITE sample of 4534 galaxies and clusters which has good angular coverage. Hence it is a good sample to study large angle anisotropies in the Hubble expansion. They found the data to exhibit dipole structure (both in Local Group and CMB frames) of which amplitude is dependent on distance. Ref. [84] studied the matter further by investigating also quadrupole anisotropies in the Hubble flow. They found that observations suggest both dipole and quadrupole are anisotropic at high confidence for redshifts smaller than ~ 0.045. Furthermore, they found the best fit flat ΛCDM model to be compatible with the Hubble dipole if the boost of the frame of the Local Group with respect to the CMB frame is approximately

350 km/s; this is only half of the boost required in order to explain the CMB dipole by the peculiar velocity alone. They continued by studying axisymmetric Szekeres models that are inhomogeneous for r smaller than $\sim 100h^{-1}Mpc$ and coincide with the ΛCDM at that limit. They found the Szekeres model, which effectively exhibits the Local Void and the Great Attractor, to give a better fit for the Hubble dipole than the ΛCDM model with peculiar velocity. However, the quadrupole predicted by the Szekeres model was too small in comparison with the observations.

4.2.2 Baryon acoustic oscillations

As mentioned earlier, the low redshift BAO observations are in good agreement with the ΛCDM model. BAO data have been tested against the LTB models by several authors and with conflicting results. The discrepancy, however, might have a simple explanation: the studies using BAO data from wider redshift range [61, 68, 60] found more tension between the data and the LTB model than those exploring data from a narrower range [57, 59]. In Ref. [2] is further studied the conjecture that wider redshift range brings more tension between BAO and the LTB models.

The high redshift BAO ($z > 2$) data obtained from the Lyman-α forest [85, 86] exhibits incompatibility with the ΛCDM model [33]. This issue was confronted with the LTB models for the first time in [2] and the results will be presented in Section 5.2.

4.2.3 Cosmic microwave background

Several unlikely features have been observed in the CMB, albeit their significance is under a debate. In this section, some of the anomalies are first introduced and then later some approaches aiming to resolve the anomalies are presented. A more comprehensive review of the anomalies is given in Ref. [87].

Lack of power of the lowest multipole moments

The missing power of the lowest multipole moments, the most significant on the quadrupole, was first reported by COBE (due to observational limitations it was not considered significant) and then confirmed by WMAP [88]. This was confirmed also by Planck and the present estimate for the p-value from the Planck data for the occurrence of the low variance of low

multipoles is $\leq 0.5\%$ [89], when the ΛCDM model is taken as the zero hypothesis.

Lack of angular two-point correlation of the largest scales

Unexpectedly low two-point correlation for scales larger than about 60% was also first discovered by COBE and then confirmed by WMAP [88] and Planck [89]. The significance of this anomaly depends on the used mask and statistical methods [87], but assuming the ΛCDM model the p-values of the observed two-point correlations for the large angular scales are at most some per cents [89].

Planarity and alignment of the quadru- and octopoles

In Ref. [90] the authors demonstrated that the octopole moment is unexpectedly planar with a p-value $\sim 5\%$. Furthermore, the authors found another feature that is even more unexpected: the normal to the quadrupole is anomalously well aligned with the preferred axis exhibited by the octopole "plane" (p-value $\sim 1.5\%$). The quadrupole moment is necessary planar and therefore it has a well-defined normal. The octopole moment is almost planar and its preferred axis, analogous to its normal, cannot be unambiguously determined but various different methods have been applied [87]. What is notable is that these anomalies appear to persist independently on the used map or the statistical method in both WMAP and Planck data, and in fact, further anomalous alignments have discovered as the preferred axes of quadrupoles and octopoles appear to be also aligned with the dipole momentum of the CMB and the normal to the Ecliptic plane [87]. The most resent evaluation for the significance of the quadrupole-octopole alignment has p-value $\leq 0.5\%$ [91].

Cold spot

Departure from Gaussianity on the CMB was first reported using first-year WMAP data in Ref. [92], where a non-Gaussian signal was detected on the southern hemisphere at scales corresponding to $\sim 10^\circ$ in the sky. The authors of Ref. [93] discovered the non-Gaussianity to be induced by a cold spot on a southern hemisphere as the CMB map becomes compatible with Gaussianity after excluding this spot. Furthermore, they report the probability of such a cold spot to exist in a Gaussian model is about $\sim 0.2\%$.

The most resent evaluation for the significance of the anomaly is evaluated in Ref. [89], where the corresponding p-value is found to be $\leq 1.0\%$.

Hemispherical power asymmetry

The amplitudes of the large scale fluctuations between opposite hemispheres were compared with each other in Ref. [94] and unexpected asymmetry was discovered. The maximum asymmetry was found when the opposing hemispheres are close to those defined by the ecliptic plane, albeit it is somewhat dependent on the used multipoles. The power spectrum is unexpectedly low on the northern hemisphere and unexpectedly high on the southern hemisphere so that the ratio of the powers of the northern and southern hemispheres is low at 3 σ level. Presently, the asymmetry is considered unexpected at the level of p-value $\leq 0.1\%$ [89]. Alternative methods of describing the hemispherical asymmetry have also been presented, like the so-called dipolar modulation [95].

Resolutions

The LTB voids have been considered alleviating the anomalous alignment of the lowest multipoles in the CMB, in particular, the effect was presumed to emerge when the observer is removed from the symmetry centre [63]. As expected, they found that increasing the displacement also increased the amplitudes of the multipoles. However, the growth of the amplitudes of the quadrupoles and octopoles as a function of the displacement is not strong enough compared with the growth of the dipole amplitude: when the dipole amplitude reached its maximum amplitude (order of 10^{-3}), the quadrupole is of order 10^{-7} and the octopole is of order 10^{-9}. Therefore, the quadrupoles and octopoles induced by displacement from the symmetry centre in a giant void can hardly explain the low l multipole alignment, which is a observed anisotropy of the order 10^{-5}. Furthermore, the authors concluded that even if a giant void and peculiar motion are both taken into account, the alignment remains without an explanation: if the observer has enough velocity in the right direction so that the displacement can be increased to bring the dipole and quadrupole amplitudes to the correct order, the octopole still remains too small.

In Ref. [96], the type VII_h Bianchi model is compared with the first year data of WMAP on large angular scales ($l \leq 64$). They apply the formalism

of Ref. [97], where the models are sourced by dust and characterised by the parameters Ω_m, x, and handedness. Here, Ω_m is the energy density of dust today and $x = \sqrt{h/(1-\Omega_m)}$, where h gives the scale where the basis vectors changes orientation. In addition, Ω_m is subject to the constraint $\Omega_m + \Omega_k = 1$, where Ω_k is the present curvature density. These models contain a preferred axis: the basis changes its orientation with respect to the preferred axis and Ω_m is related to the asymmetry along the preferred axis. Ref. [96] finds the best fit model to be right-handed and have

$$x = 0.55, \quad \Omega_m = 0.5, \quad \Sigma = 2.4 \times 10^{-10}, \quad \mathcal{V} = 4.3 \times 10^{-10},$$

where all the quantities represent their present day values. Effectively, their Bianchi models arise so that the excess power of the southern hemisphere over the northern hemisphere stipulates low Ω_m whereas the cold spot and its surrounding structure is responsible for the x value. They continue the investigation by creating a "Bianchi-corrected" CMB sky map by removing the best fit Bianchi sky map from the original WMAP sky map. Their statistical analysis of the Bianchi-corrected data shows that the best fit parameter values are sufficient to reduce the significance of the hemispherical power asymmetry into a non-anomalous level and resolve the cold spot anomaly. In addition, the quadrupole amplitude in the Bianchi-corrected data is no longer unexpectedly low as in the original WMAP data and the quadrupole and octopole are no longer aligned with each other. That is, they were able to dissipate four anomalies, but at the cost of $\Omega_k = 0.5$. On the other hand, they used the method given in Ref. [97], which dates back to the time when dark energy was not considered as part of the energy density of the universe and dust was considered as the dominating component.

The type VII_h Bianchi model was further studied in Ref. [98], now including dark energy. The authors of Ref. [98] extended the formalism of Ref. [97] by inserting the cosmological constant Λ in the equations, which expands the parameter space of that used in Ref. [96] by Ω_Λ. The main result of Ref. [98] is that there is a number of members in the three-dimensional parameter space $(\Omega_m, \Omega_\Lambda, x)$ so that each member manifests a similar Bianchi-corrected structure as the best fit model in Ref. [98], but none of the members is compatible with other cosmological observations (the results are confirmed by Ref. [99]). The Bianchi-corrected structure in question includes geodesic focusing and spiral turns, which create hemispherical asymmetry and hot or cold spots [97, 96]. The authors of Ref. [98]

discussed also dynamical dark energy models and reasoned them to result in a similar outcome as the present values of dark energy and curvature density appear more significant than the preceding dynamics.

In addition to the above proposed settlements, a number of other approaches have also been taken in order to explain the anomalies, like elongated local voids [100], anisotropic inflation [101, 102], and imperfect dark energy [103, 104, 105, 106, 107]. The anomalies of the CMB, however remain unexplained hence providing the motivation for paper [3].

Chapter 5

Summary of papers

The cosmological principle is relaxed in papers [1, 2, 3, 4] in order to investigate the effects of inhomogeneity and anisotropy in cosmology. In papers [1, 4] we examined if the present observer's luminosity distance is converging to an asymptotic curve and furthermore, is already very close to it. This would imply lack of information about the initial conditions of the universe, in particular, a family of bang time functions would lead the luminosity distance to converge to the same asymptotic curve. By picking up the most homogeneous $t_b(r)$ of this family we refer to as homogenising the system and conjecture this dispels the fine-tuning issue and some of the observational discrepancies discussed in Section 4.1.1. In [2] we examine some of the discrepancies between observations and the LTB models in detail. In [3] we take a step towards non-perfect fluid Bianchi cosmology by investigating a specific model. This is motivated by the unexplained anisotropies in the CMB, discussed in Sections 4.2.1 and 4.2.3.

5.1 Homogenising inhomogeneous models

As discussed in Section 4.1.1, some of the observations, like SNIa, prefer inhomogeneity whereas some of the observations, like kSZ, prefer homogeneity. Furthermore, the fine-tuning issue of the observer's location is caused by the inhomogeneity. We studied in papers [1, 4] if these apparently conflicting preferences vanish by considering some unusual configuration of inhomogeneities. In practice, we took a SNIa compatible ΛLTB model and examined if it can be homogenised.

The idea for homogenising inhomogeneous models is introduced in [1, 4] and goes as follows. Let us denote the luminosity distance of the Fried-

mannian model by $D_L^F(z)$ and assume that the present observer sees the luminosity distance $D_L^F(z) + \delta D_L(z)$, where

$$|\delta D_L| \ll D_L^F(z) \tag{5.1}$$

for some range of redshift, say when $z \in [0, 1.2]$. Furthermore, let us assume $\delta D_L(z)$ is observationally indistinguishable when $z \in [0, 1.2]$. Consequently, the future observer cannot distinguish the evolving of the luminosity distance, if

$$\lim_{t_0 \to \infty} \delta D_L(z) = 0, \tag{5.2}$$

and $z \in [0, 1.2]$. On the other hand, the present observer cannot tell how far in the past $\delta D_L(z)$ has been below observational limits and hence have no information on the initial conditions of the universe at $z \in [0, 1.2]$.[1] The form of the bang time function $t_b(r)$ of the inhomogeneous model is therefore out of reach of the present observer and in fact, there is a family of functions $t_b(r)$ which lead the luminosity distance of the system to approach D_L^F. Selecting the most homogeneous function t_b of the family we refer to as homogenising the system. It is notable that homogenising the model should make it also older in the process: making the universe older suggests it is closer to the asymptote, whereas making it younger suggests it is further away from the asymptote and $\delta D_L(z)$ may no longer be indistinguishable.

In paper [1] we proposed the condition (5.2) takes place when

$$\lim_{t_0 \to \infty} \frac{dz}{dt_0} = 0, \tag{5.3}$$

that is, the redshift drift[2] dz/dt_0 converges to zero as the observer's time $t_0 \to \infty$. The redshift drift was first introduced in Ref. [111] within the Friedmann models. The authors of Ref. [112] were the first to derive the redshift drift equation for the LTB models. In [1] we presented an alternative derivation, discussed the meaning of the condition (5.3) within the ΛLTB models and analysed the ΛCDM model. The analysis revealed the condition (5.3) cannot hold but for one non-zero z per a null geodesic and

[1] The situation is analogous to a physical system, where the system has reached a stable state thus hiding its initial state.

[2] The redshift drift is observationally achievable for us in the next generation surveys, see [108, 109, 110]. However, here we employ the theoretical aspects it provides.

the distance r, for which the condition holds, changes in time. Thus, the luminosity distance cannot converge to a constant value for any observable. Of course, this analysis was only an exercise before proceeding to more cumbersome cases; the result was expected as the alternative would imply the absurdity of homogenising a homogeneous model.

In Ref. [4] we continued the study further by thoroughly scrutinising the ΛLTB model. We extracted three separate cases which can satisfy the condition (5.3):

I The static universe, where the expansion freezes both in radial and angular directions (R and $R_{,r}$ tend to a constant for each r).

II The big universe, where the expansion in the angular direction has grown large enough.

III The bizarre universe, where the scales grow in the angular direction and crunch in the radial direction.

After fixing the gauge, the ΛLTB models contain two free functions which need to be fixed in order to close and solve the system. Demanding the model to be compatible with SNIa data fixes one of them, we imposed $D_L = D_L^F$. Moreover, we imposed $dz/dt_0 \approx 0$ implying Eq. (5.1) is satisfied. Consequently, what was left to do was to solve the system and check whether Eq. (5.2) holds.

We solved the system for different values of Λ and found that each solution belongs in Case I. Further analysis showed that Eq. (5.2) does not hold for any Λ and the luminosity distance before and after the homogenising procedure distinctly differs from each other. The fact that we find solutions using constraint $dz/dt_0 \approx 0$ but still Eq. (5.2) does not hold implies that the condition $dz/dt_0 \approx 0$ holds only momentarily. This is similar to that found in [1] when investigating the ΛCDM model, where $dz/dt_0 = 0$ can hold only for one r per a null geodesic and the distance r is not the same for different null geodesics. The difference between this and the ΛLTB model is that in the latter case the inhomogeneous degrees of freedom allows to set $dz/dt_0 = 0$ simultaneously for a range of distances r. The common factor between the models is that both can have $dz/dt_0 = 0$ only momentarily. On the strength of these results, we concluded the ΛLTB models cannot be homogenised.

5.2 The line of sight vs. local growth

The main purpose of [2] was to investigate which properties introduce difference between the LTB and the ΛCDM models so that observables dependent on these properties are capable pointing out the preferred model. We assumed the LTB model to be approximately homogeneous at the early times and have a constant $t_b(r)$ function. In addition, we imposed the ΛCDM luminosity distance for the LTB model, which permitted us to investigate the issue without SNIa data fitting. The analysis of the properties of these models led us to investigate observables dependent on local growth in more detail. We paid special attention to the discrepancy (discussed in more detail in Section 4.2.2) encountered when fitting void models simultaneously to the line of sight (like SNIa) and local growth (like BAO) data. We were the first ones fitting BAO data to the void model characterised by the ΛCDM luminosity distance and moreover, we were the first fitting the BAO features of the LαF within the framework of the LTB models.

Studying the properties of the LTB and ΛCDM models revealed that local expansion rates differ the most between them. This can be illustrated by the so-called relative local expansion rates (RLER), which gives a measure for the growth of scales from some early time t_e to the present null geodesic relative to the same measure at the origin. By assuming approximately homogeneous early time and defining $R(r,t) \equiv A(r,t)r$, the RLERs can be written as

$$\begin{aligned} \mathcal{R}^R &= \frac{R_{,r}[r(z),t(z)]}{R_{,r}[r(z),t_e]}A(0,t_e), \\ \mathcal{R}^T &= \frac{R[r(z),t(z)]}{R[r(z),t_e]}A(0,t_e), \\ \mathcal{R}^F &= \frac{1}{1+z}, \end{aligned} \tag{5.4}$$

where $\mathcal{R}^R$ and $\mathcal{R}^T$ are the RLERs in the radial and transverse directions in the LTB model, respectively and $\mathcal{R}^F$ is the RLER in the Friedmannian model. In addition, the Hubble functions in radial and transverse directions

$$H^R = \frac{R_{,tr}[r(z),t(z)]}{R_{,r}[r(z),t_e]}, \quad H^T = \frac{R_{,tr}[r(z),t(z)]}{R_{,r}[r(z),t_e]}, \tag{5.5}$$

respectively, exhibit considerable deviation from their Friedmannian coun-

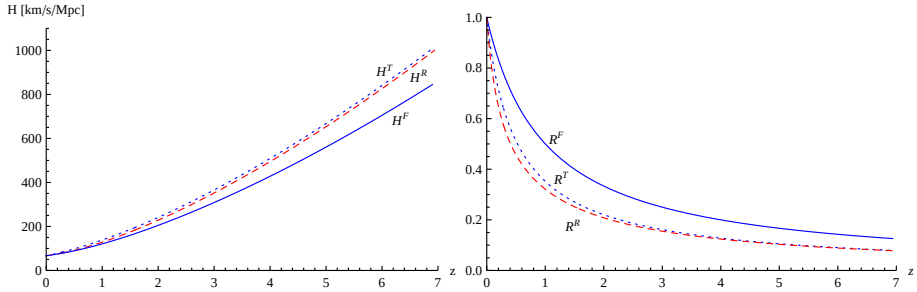

Figure 5.1: The LTB and the ΛCDM models with $H_0^F = 67.1$ and $\Omega_m^F = 0.32$. The left panel shows the radial Hubble function, $H^R(z)$ (dashed red), the transverse Hubble function, $H^T(z)$ (dotted blue), and the Hubble function of the ΛCDM model, $H^F(z)$ (solid blue). All three Hubble functions coincides at $z = 0$. The relative difference between $H^F(z)$ and $H^R(z)$ is approximately 6 % and 16 %, and the relative difference between $H^F(z)$ and $H^T(z)$ is approximately 13 % and 18 %, at redshifts 1 and 6, respectively. The right panel shows RLER's, where $\mathcal{R}^R$, $\mathcal{R}^T$ and $\mathcal{R}^F$ correspond to dashed red, dotted blue and solid blue curves, respectively. The relative difference between $\mathcal{R}^F$ and $\mathcal{R}^R$ is approximately 43 % and 47 %, and the relative difference between $\mathcal{R}^F$ and $\mathcal{R}^T$ is approximately 35 % and 45 %, at redshifts 1 and 6, respectively. Figure from [2].

terparts. The deviations are illustrated in Figure 5.1, which is taken from [2]. Clearly, for both the RLERs and Hubble functions: the wider the redshift range, the larger the difference.

On the strength of these results, we investigated BAO data, which is a measure of a local growth. The relative difference of the RLERs and the Hubble functions of the models is growing with respect to z, illustrated in Fig. 5.1, and this is transmitted to the BAO measures, as can be seen on the right panel of Fig. 5.2. This is in agreement with the conjecture presented in Section 4.2.2 that the tension between the models grows when BAO data is obtained from a wider range of redshift.

The low BAO data ($z_{eff} < 1$) in itself gives similar χ^2 values for both models, which is displayed in the left panel of Figure 5.2. However, the LTB model is clearly in more conflict with the combined SNIa and low BAO data compared with the ΛCDM model and hence the combined data set favours the ΛCDM model: the p-value imply that the LTB model is ruled out by 98 % confidence and Bayesian information condemns strong evidence against the LTB model.

The analysis of the LαF BAO data was executed with extra caution due

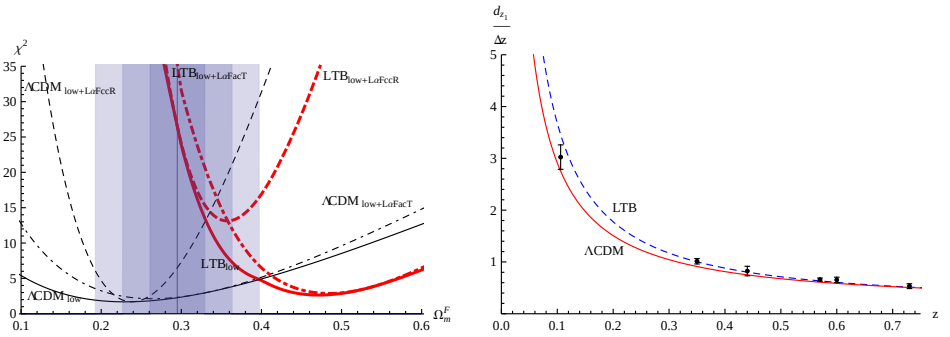

Figure 5.2: The left panel: Different $\chi^2(\Omega_m^F)$ curves for different models and data sets are presented. The black vertical line in the middle of the vertical contours indicates the preferred Ω_m^F according to the SN data [38], whereas the vertical contours indicates 1-3 σ deviations from the best fit value. The right panel: The (black) points and bars represent observations and their 1σ errors, the red solid curve represents the ΛCDM model's prediction and the dashed blue curve represent the LTB model's prediction. For both models, $\Omega_m^F = 0.32$ and Δz is chosen to correspond LαFccR. Figure from [2].

to the questioned viability of the measurements [33]: we took the BAO data of the LαF forest in the radial and transverse directions from two individual surveys [86] and [85] and investigated them separately. Thus, we did four analysis including low BAO and LαF BAO data. Two of the results are plotted in Figure 5.2, the ones that are the most favourable to the LTB models both in the radial and transverse directions. The acknowledged discrepancy between LαF data and the ΛCDM model [33] is visible in the figure. However, the incompatibility with the LTB void is even greater.

The homogeneity of the early times implies that the BAO observables have evolved from inhomogeneities of the size of the first CMB peak (or more precisely, the angular diameter of the first CMB peak at the surface of last scattering θ^*) and the analysis made for BAO data was extended to CMB data by the part of the ratio analysis. The procedure was not unambiguous, because the LTB model cannot reproduce the ΛCDM luminosity distance beyond $z \approx 7$ without hitting to a shell crossing (SC) singularity [113]. For $7 \lesssim z$, we extended the model by several functions, referred as tails, which were tailored to avoid the SC singularities and to make the system approximately homogeneous for $z \gtrsim 1000$. In addition, we ignored the effects of pressure in this analysis. The results are illustrated in Figure 5.3, where different tails are presented in the left plot and their

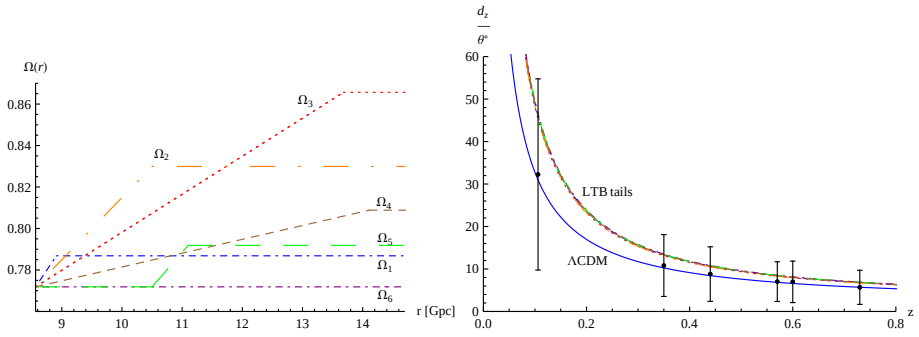

Figure 5.3: The LTB and the ΛCDM models with $H_0^F = 67.1$ and $\Omega_m^F = 0.32$. In the left panel several tails are plotted. In the right panel, (black) points and bars are observed d_z/θ^* values and their 1σ error bars, the solid blue curve represents the ΛCDM prediction and non-solid colored curves represent the LTB models with tails, the curve color and style indicates the corresponding left panel tails. The LTB curves can be arranged from the worst to the best fit as follows: Ω_6, Ω_5, Ω_1, Ω_4, Ω_2, and Ω_3. Figure from [2].

corresponding ratio curves are drawn together with the ΛCDM ratio curve and the data points in the right plot. The LTB curves on the right plot are indistinguishable from each other indicating that chancing the tail has insignificant impact. The better fit of the ΛCDM model is striking even though the curves corresponding the LTB models are inside the 1σ error bars. In addition to the tails presented in the figure, we considered more complex functions as tails and allowed them to start at lower redshifts[3] ($z \approx 2$), but no significant improvement was found. The better fit of the ΛCDM model is so striking that it is hard to believe the presence of pressure would change it.

5.3 Anisotropic acceleration and non-perfect fluid

Paper [3] was devoted for studying the tilted axisymmetric type IX Bianchi model presented in Section 2.4.4. The aim was to analyse the phase space of the model by employing the dynamical systems analysis [19] and study the cosmological applicability of the model.

[3]The luminosity distance with respect to the redshift is considered well known only up to $z \approx 2$, therefore it is sufficient that the luminosity distance of the LTB model is equal to D_L^F only up to $z \approx 2$.

The dynamics of the system is described by Eqs. (2.127), (2.128), (2.129), and (2.130), which are subject to the constraint (2.131). We employ parameter ϵ as an indicator of cosmological applicability: $\epsilon < 1$ indicates acceleration, $\epsilon > 1$ indicates deceleration and furthermore, from Eqs. (2.132) and (2.133) can be seen that

$$\begin{aligned}
\epsilon &= 1 && \text{in the curvature filled universe}\,,\\
\epsilon &= 3 && \text{in the shear filled universe}\,,\\
\epsilon &= 2 - \frac{1}{1+\operatorname{sech}(2\lambda)} && \text{in the dust filled universe}\,,\\
\epsilon &= 2 && \text{in the radiation filled universe}\,,\\
\epsilon &= 0 && \text{in the dark energy filled universe}\,.
\end{aligned}$$

By treating λ and w as constant parameters and eliminating the dynamical equation for the curvature using the constraining Eq. (2.131), we analysed the three-dimensional phase space $(\Omega, \Sigma, \mathcal{V})$. The system has seven fixed points and we investigated their cosmological applicability by evaluating their stability and the value of ϵ in the (w, λ) parameter space. Several interesting aspects arose and was discussed, like the shear-free conditions, the role of universal rotation, and the freezing effect due to $\cosh\lambda \gg 1$. However, the most interesting possibilities arose from the fixed point

$$\begin{aligned}
\mathcal{V}^* &= 0\\
K^* &= 0\\
\Omega^* &= \frac{3(w-1)(3w-4W+1)}{W(-3w+2W+1)^2}\\
\Sigma^* &= \frac{2-2W}{-3w+2W+1}
\end{aligned} \tag{5.6}$$

which allows for anisotropically accelerating stable solutions (the superscript $*$ denotes that the quantity is evaluated at a fixed point). The fixed point has non-zero shear if $w \neq -1$ and $\lambda \neq 0$ ($\Rightarrow W \neq 1$) and then consulting Figure 5.4, we find stable anisotropic acceleration to occur when $0 < \lambda$ and $w \lesssim -1$.

The anisotropic feature of the fixed point exhibits a counter example to the cosmic no-hair conjecture by Wald [28]. The conjecture is based on a theorem which assumes nothing else from the energy-momentum tensor except it has to comply with the dominant and strong energy conditions.

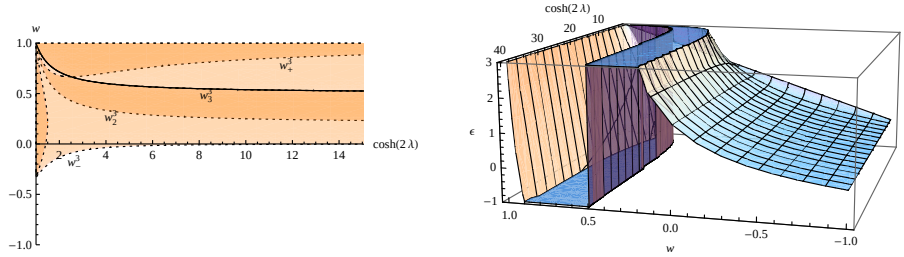

Figure 5.4: The left panel shows the stability properties of the fixed point (5.6). In the white region the fixed point is an attractor, and a saddle point in the orange regions (repelling in one direction in the lighter and two directions in the darker shaded areas). On the black curves the fixed point is not defined, and on the dotted curves (including $w = 0$) a Lyaponov exponent has a vanishing real part. If $\lambda \to \infty$, then $w_+^3 \to 1$, $w_3^3 \to 1/2$, $w_2^3 \to 1/5$ and $w_-^3 \to 0$. The right panel shows the values of ϵ. Figure from [3].

The accelerated expansion in the theorem is induced by Λ, which of course do violate the aforementioned energy conditions, but is excluded from the energy-momentum tensor. In our paper, this would coincide with the assumption that $w = -1$. Therefore, the difference between ours and Wald's paper is that we promoted Λ to be a tilted fluid which does not necessarily implement the equation of state $p = -\rho$. This simple difference results in qualitatively remarkably different solutions.

The extensive numerical analysis of anisotropic late time cosmology was executed, where the system undergoes the radiation and matter dominated epochs and then converges towards the dark energy dominated state given by the attracting fixed point (5.6). This was executed by decomposing the effective energy momentum tensor to dark energy, dust and radiation components so that one of the fluids is tilted with respect to the frame of reference whereas two of them are comoving with it. The main result of the analysis is that taking the present-day energy density values to be $\Omega_\Lambda \approx 0.7$ and $\Omega_d \approx 0.3$ and $\Omega_r \sim 10^{-5}$, the vorticity can easily reach the value $\mathcal{V} \sim 10^{-5}$ today. This is the same order of magnitude as where the anomalies of the CMB appear. Moreover, the only fine-tuning a viable late time cosmology requires here is that the curvature is small enough at the beginning of the radiation dominated era. This is the same fine-tuning issue as the ΛCDM model has without inflation.

5.4 Conclusions and outlook

It is interesting to find out whether the cosmological observations become ever so accurate that we are forced to discard the cosmological principle. In order to find this out, the effects of inhomogeneity needs to be understood beyond that of the standard perturbation theory. The studies so far have shown that violating the cosmological principle introduces benefits and drawbacks; we should take them as guiding lessons towards more realistic modelling.

The spherically symmetric LTB models are hardly realistic descriptions of our universe, but they offer valuable information about the effects of radial inhomogeneity. For example, the results of the paper [2] imply that the discrepancy between the ΛCDM model and the BAO features of the LαF is not caused by a giant spherical void (where Earth is at the symmetry centre). On the other hand, the results show that inhomogeneity has an impact on the matter and therefore other type of inhomogeneity might viably explain the incompatibility between data and modelling. Therefore, more sophisticated models, like those composed of voids and overdense regions (e.g. Refs. [66, 67]) might alleviate the tension.

On the other hand, inhomogeneities can introduce unexpected features, for example the observed luminosity distance will no longer change in time like in the Friedmann models. The results of the papers [1, 4] state that our luminosity distance is not close to a attracting curve, or if it is, the feature is not enclosed by the ΛLTB models. Indeed, these models are merely another step towards the realistic description of the universe and each step should be carefully investigated in order to discover their effects. The fact that the feature suggested and studied in [1, 4] is not enclosed by the ΛLTB models, does not imply the absence of the feature in more general and realistic models. The method can be applied to more general models.

The properties of the phase space of the tilted Bianchi models have been extensively studied [114, 115, 116, 117, 118, 119, 19] but the non-perfect fluid cases are not well known. Furthermore, observations are unable to rule out dark energy that violates the cosmological principle, which gives the physical motivation for examining non-perfect dark energy fluids [106]. The difference in phenomenology between perfect and non-perfect fluid descriptions may be significant. Assuming the cosmic fluid to be tilted perfect fluid, the maximum amount of vorticity in the present universe is less than

$\sim 10^{-10}$ in the most general Bianchi types IX and VII$_h$. As the anomalies in the CMB are of the order 10^{-5}, the vorticity cannot dispel any of the anomalies by itself. By discarding the assumption of tilted perfect fluid and allowing the energy content of the universe to experience energy conduction, we showed in [3] that the amount of vorticity can easily be increased to the present value $\mathcal{V} \sim 10^{-5}$. The vorticity could then alleviate some anomalies. In addition, it could also be beneficial to reanalyse the studies of type VII$_h$ Bianchi models which failed to dissipate the anomalies by assuming perfect fluid, now by assuming non-perfect fluid.

On the other hand, sufficient amount of shear and vorticity should survive the inflation for the above scenario to take place. Such inflationary model have not been presented so far. Therefore, in order to harness the full explaining power of the Bianchi models, an inflation model with a hint of shear and vorticity should be constituted. Furthermore, such anisotropic inflation could mix even quite simple initial conditions to give much more flavorful output than the standard description and alleviate some of the anomalies in itself.

Bibliography

[1] P. Sundell and I. Vilja, "Inhomogeneous cosmological models and fine-tuning of the initial state," *Mod. Phys. Lett.*, vol. A29, no. 10, p. 1450053, 2014.

[2] P. Sundell, E. Mörtsell, and I. Vilja, "Can a void mimic the Λ in ΛCDM?" *JCAP*, vol. 1508, p. 037, 2015.

[3] P. Sundell and T. Koivisto, "Anisotropic cosmology and inflation from a tilted Bianchi IX model," *Phys. Rev.*, vol. D92, no. 12, p. 123529, 2015.

[4] P. Sundell and I. Vilja, "Inhomogeneity of the ΛLTB models," *arXiv:1601.05256*, 2016.

[5] A. Einstein, "Cosmological Considerations in the General Theory of Relativity," *Sitzungsber. Preuss. Akad. Wiss. Berlin (Math. Phys.)*, vol. 1917, pp. 142–152, 1917.

[6] A. Einstein, *The Collected Papers of Albert Einstein, Volume 6: The Berlin Years: Writings, 1914-1917.*, 1996.

[7] M. A. H. MacCallum, "Milestones of general relativity: Hubble's law (1929) and the expansion of the universe," *Class. Quant. Grav.*, vol. 32, no. 12, p. 124002, 2015.

[8] W. de Sitter, "On Einstein's Theory of Gravitation and its Astronomical Consequences. Third Paper." *Mon. Not. Roy. Astron. Soc.*, vol. 78, no. 1, pp. 3–28, 1917. [Online]. Available: http://mnras.oxfordjournals.org/content/78/1/3.short

[9] A. Friedmann, "On the Curvature of space," *Z. Phys.*, vol. 10, pp. 377–386, 1922, [Gen. Rel. Grav.31,1991(1999)].

[10] A. Friedmann, "On the Possibility of a world with constant negative curvature of space," *Z. Phys.*, vol. 21, pp. 326–332, 1924, [Gen. Rel. Grav.31,2001(1999)].

[11] J.-P. Luminet, "Lemaitre's Big Bang," *arxiv:1503.08304*, 2015.

[12] G. Lemaître, "Republication of: A homogeneous universe of constant mass and increasing radius accounting for the radial velocity of extra-galactic nebulae," *Gen. Rel. Grav.*, vol. 45, no. 8, pp. 1635–1646, 2013. [Online]. Available: http://dx.doi.org/10.1007/s10714-013-1548-3

[13] E. Hubble, "A relation between distance and radial velocity among extra-galactic nebulae," *Proc. Nat. Acad. Sci.*, vol. 15, pp. 168–173, 1929.

[14] R. Durrer, "The cosmic microwave background: the history of its experimental investigation and its significance for cosmology," *Class. Quant. Grav.*, vol. 32, no. 12, p. 124007, 2015. [Online]. Available: http://stacks.iop.org/0264-9381/32/i=12/a=124007

[15] A. A. Penzias and R. W. Wilson, "A Measurement of Excess Antenna Temperature at 4080 Mc/s." *Astrophys. J.*, vol. 142, pp. 419–421, jul 1965.

[16] P. Szekeres, *A Course in Modern Mathematical Physics.* Cambridge University Press, 2004, cambridge Books Online. [Online]. Available: http://dx.doi.org/10.1017/CBO9780511607066

[17] G. F. R. Ellis, R. Maartens, and M. A. H. MacCallum, *Relativistic Cosmology.* Cambridge, UK: Cambridge University Press, Mar. 2012. [Online]. Available: http://adsabs.harvard.edu/cgi-bin/nph-bib_query?bibcode=2012reco.book.....E

[18] S. Weinberg, *Gravitation and Cosmology: Principles and Applications of the General Theory of Relativity.* New York, NY: Wiley, 1972. [Online]. Available: https://cds.cern.ch/record/100595

[19] J. Wainwright and G. F. R. Ellis, Eds., *Dynamical Systems in Cosmology.* Cambridge University Press, 1997, cambridge Books Online. [Online]. Available: http://dx.doi.org/10.1017/CBO9780511524660

[20] S. M. Carroll, "Lecture notes on general relativity," *arxiv:9712019*, 1997.

[21] M. F. Shirokov and I. Z. Fisher, "Isotropic Space with Discrete Gravitational-Field Sources. On the Theory of a Nonhomogeneous Isotropic Universe," Soviet Ast., vol. 6, p. 699, apr 1963.

[22] T. Buchert, "On average properties of inhomogeneous fluids in general relativity. 1. Dust cosmologies," *Gen. Rel. Grav.*, vol. 32, pp. 105–125, 2000.

[23] S. Räsänen, "Light propagation in statistically homogeneous and isotropic universes with general matter content," *JCAP*, vol. 2010, no. 03, p. 018, 2010. [Online]. Available: http://stacks.iop.org/1475-7516/2010/i=03/a=018

[24] G. Lemaître, "The expanding universe," *Gen. Rel. Grav.*, vol. 29, pp. 641–680, 1997.

[25] R. C. Tolman, "Effect Of Inhomogeneity On Cosmological Models," *Proc. Nat. Acad. Sci.*, vol. 20, p. 169, 1934.

[26] H. Bondi, "Spherically symmetrical models in general relativity," *Mon. Not. Roy. Astron. Soc.*, vol. 107, pp. 410–425, 1947.

[27] C. W. Misner, "Mixmaster universe," *Phys. Rev. Lett.*, vol. 22, pp. 1071–1074, 1969.

[28] R. M. Wald, "Asymptotic behavior of homogeneous cosmological models in the presence of a positive cosmological constant," *Phys. Rev.*, vol. D28, pp. 2118–2120, 1983.

[29] R. Brandenberger, "Initial Conditions for Inflation - A Short Review," 2016.

[30] G. N. Remmen and S. M. Carroll, "How Many e-Folds Should We Expect from High-Scale Inflation?" *Phys. Rev.*, vol. D90, no. 6, p. 063517, 2014.

[31] M. A. Amin, M. P. Hertzberg, D. I. Kaiser, and J. Karouby, "Nonperturbative Dynamics Of Reheating After Inflation: A Review," *Int. J. Mod. Phys.*, vol. D24, p. 1530003, 2014.

[32] P. Ade *et al.*, "Planck 2013 results. XVI. Cosmological parameters," *Astron. Astrophys.*, vol. 571, p. A16, 2014.

[33] P. A. R. Ade *et al.*, "Planck 2015 results. XIII. Cosmological parameters," *arxiv:1502.01589*, 2015.

[34] D. H. Weinberg, M. J. Mortonson, D. J. Eisenstein, C. Hirata, A. G. Riess, and E. Rozo, "Observational probes of cosmic acceleration," Phys. Rep., vol. 530, pp. 87–255, Sep. 2013.

[35] G. F. R. Ellis, "On the definition of distance in general relativity: I. M. H. Etherington (Philosophical Magazine ser. 7, vol. 15, 761 (1933))," *Gen. Rel. Grav.*, vol. 39, pp. 1047–1052, Jul. 2007.

[36] A. G. Riess *et al.*, "Observational evidence from supernovae for an accelerating universe and a cosmological constant," *Astron. J.*, vol. 116, pp. 1009–1038, 1998.

[37] S. Perlmutter *et al.*, "Measurements of Omega and Lambda from 42 high redshift supernovae," *Astrophys. J.*, vol. 517, pp. 565–586, 1999.

[38] M. Betoule *et al.*, "Improved cosmological constraints from a joint analysis of the SDSS-II and SNLS supernova samples," *Astron. Astrophys.*, vol. 568, p. A22, 2014.

[39] A. G. Riess, L. Macri, S. Casertano, H. Lampeitl, H. C. Ferguson, A. V. Filippenko, S. W. Jha, W. Li, and R. Chornock, "A 3% Solution: Determination of the Hubble Constant with the Hubble Space Telescope and Wide Field Camera 3," *Astrophys. J.*, vol. 730, p. 119, Apr. 2011.

[40] A. G. Riess *et al.*, "A 2.4% Determination of the Local Value of the Hubble Constant," *arxiv:1604.01424*, 2016.

[41] G. Efstathiou, "H0 Revisited," *Mon. Not. Roy. Astron. Soc.*, vol. 440, no. 2, pp. 1138–1152, 2014.

[42] C. Baltay, "The accelerating universe and dark energy," *Int. J. Mod. Phys.*, vol. D23, no. 06, p. 1430012, 2014. [Online]. Available: http://www.worldscientific.com/doi/abs/10.1142/S0218271814300122

[43] F. Beutler, C. Blake, M. Colless, D. H. Jones, L. Staveley-Smith, L. Campbell, Q. Parker, W. Saunders, and F. Watson, "The 6dF Galaxy Survey: baryon acoustic oscillations and the local Hubble constant," *Mon. Not. Roy. Astron. Soc.*, vol. 416, pp. 3017–3032, Oct. 2011.

[44] N. Padmanabhan, X. Xu, D. J. Eisenstein, R. Scalzo, A. J. Cuesta, K. T. Mehta, and E. Kazin, "A 2 per cent distance to z = 0.35 by reconstructing baryon acoustic oscillations - I. Methods and application to the Sloan Digital Sky Survey," *Mon. Not. Roy. Astron. Soc.*, vol. 427, pp. 2132–2145, Dec. 2012.

[45] L. Anderson *et al.*, "The clustering of galaxies in the SDSS-III Baryon Oscillation Spectroscopic Survey: baryon acoustic oscillations in the Data Release 9 spectroscopic galaxy sample," *Mon. Not. Roy. Astron. Soc.*, vol. 427, pp. 3435–3467, Dec. 2012.

[46] C. Blake *et al.*, "The WiggleZ Dark Energy Survey: mapping the distance-redshift relation with baryon acoustic oscillations," *Mon. Not. Roy. Astron. Soc.*, vol. 418, pp. 1707–1724, Dec. 2011.

[47] G. Hinshaw *et al.*, "Nine-year Wilkinson Microwave Anisotropy Probe (WMAP) Observations: Cosmological Parameter Results," ApJS, vol. 208, p. 19, Oct. 2013.

[48] A. J. Ross, L. Samushia, C. Howlett, W. J. Percival, A. Burden, and M. Manera, "The clustering of the SDSS DR7 main Galaxy sample – I. A 4 per cent distance measure at $z = 0.15$," *Mon. Not. Roy. Astron. Soc.*, vol. 449, no. 1, pp. 835–847, 2015.

[49] L. Anderson *et al.*, "The clustering of galaxies in the SDSS-III Baryon Oscillation Spectroscopic Survey: baryon acoustic oscillations in the Data Releases 10 and 11 Galaxy samples," *Mon. Not. Roy. Astron. Soc.*, vol. 441, no. 1, pp. 24–62, 2014.

[50] T. Buchert, A. A. Coley, H. Kleinert, B. F. Roukema, and D. L. Wiltshire, "Observational Challenges for the Standard FLRW Model," *Int. J. Mod. Phys.*, vol. D25, no. 03, p. 1630007, 2016.

[51] S. Weinberg, "The Cosmological constant problems," in *Sources and detection of dark matter and dark energy in the universe. Proceedings,*

4th International Symposium, DM 2000, Marina del Rey, USA, February 23-25, 2000, 2000, pp. 18–26. [Online]. Available: http://www.slac.stanford.edu/spires/find/books/www?cl=QB461:I57:2000

[52] J. Yoo and Y. Watanabe, "Theoretical Models of Dark Energy," *Int. J. Mod. Phys.*, vol. D21, p. 1230002, Dec. 2012.

[53] E. Bianchi and C. Rovelli, "Why all these prejudices against a constant?" 2010.

[54] P. A. R. Ade *et al.*, "Planck 2015 results. XIV. Dark energy and modified gravity," *arxiv:1502.01590*, 2015.

[55] M.-N. Celerier, "Do we really see a cosmological constant in the supernovae data?" *Astron. Astrophys.*, vol. 353, pp. 63–71, 2000.

[56] H. Alnes, M. Amarzguioui, and O. Gron, "An inhomogeneous alternative to dark energy?" *Phys. Rev.*, vol. D73, p. 083519, 2006.

[57] J. García-Bellido and T. Haugbølle, "Confronting Lemaitre-Tolman-Bondi models with Observational Cosmology," *JCAP*, vol. 0804, p. 003, 2008.

[58] M. Blomqvist and E. Mörtsell, "Supernovae as seen by off-center observers in a local void," *JCAP*, vol. 5, p. 006, May 2010.

[59] T. Biswas, A. Notari, and W. Valkenburg, "Testing the Void against Cosmological data: fitting CMB, BAO, SN and H0," *JCAP*, vol. 1011, p. 030, 2010.

[60] M. Zumalacárregui, J. García-Bellido, and P. Ruiz-Lapuente, "Tension in the void: cosmic rulers strain inhomogeneous cosmologies," *JCAP*, vol. 10, p. 009, Oct. 2012.

[61] M. Redlich, K. Bolejko, S. Meyer, G. F. Lewis, and M. Bartelmann, "Probing spatial homogeneity with LTB models: a detailed discussion," *Astron. Astrophys.*, vol. 570, p. A63, 2014.

[62] M. Ishak, J. Richardson, D. Whittington, and D. Garred, "Dark Energy or Apparent Acceleration Due to a Relativistic Cosmological Model More Complex than FLRW?" *Phys. Rev.*, vol. D78, p. 123531, 2008, [Erratum: Phys. Rev.D84,089902(2011)].

[63] H. Alnes and M. Amarzguioui, "CMB anisotropies seen by an off-center observer in a spherically symmetric inhomogeneous Universe," *Phys. Rev.*, vol. D74, p. 103520, 2006.

[64] K. Bolejko and R. A. Sussman, "Cosmic spherical void via coarse-graining and averaging non-spherical structures," *Phys. Lett.*, vol. B697, pp. 265–270, 2011.

[65] R. G. Buckley and E. M. Schlegel, "Cmb dipoles and other low-order multipoles in the quasispherical szekeres model," *Phys. Rev.*, vol. D87, p. 023524, Jan 2013. [Online]. Available: http://link.aps.org/doi/10.1103/PhysRevD.87.023524

[66] R. A. Sussman and I. Delgado Gaspar, "Multiple nonspherical structures from the extrema of Szekeres scalars," *Phys. Rev.*, vol. D92, no. 8, p. 083533, 2015.

[67] R. A. Sussman, I. D. Gaspar, and J. C. Hidalgo, "Coarse-grained description of cosmic structure from Szekeres models," *JCAP*, vol. 1603, no. 03, p. 012, 2016.

[68] A. Moss, J. P. Zibin, and D. Scott, "Precision cosmology defeats void models for acceleration," *Phys. Rev.*, vol. D83, no. 10, p. 103515, May 2011.

[69] J. García-Bellido and T. Haugbølle, "Looking the void in the eyes - the kSZ effect in LTB models," *JCAP*, vol. 0809, p. 016, 2008.

[70] A. Krasiński, "Accelerating expansion or inhomogeneity? A comparison of the ΛCDM and Lemaître-Tolman models," *Phys. Rev.*, vol. D89, no. 2, p. 023520, 2014, [Erratum: Phys. Rev.D89,no.8,089901(2014)].

[71] T. Clifton, P. G. Ferreira, and J. Zuntz, "What the small angle CMB really tells us about the curvature of the Universe," *JCAP*, vol. 0907, p. 029, 2009.

[72] P. Bull, T. Clifton, and P. G. Ferreira, "The kSZ effect as a test of general radial inhomogeneity in LTB cosmology," *Phys. Rev.*, vol. D85, p. 024002, 2012.

[73] V. Marra and M. Paakkonen, "Observational constraints on the LLTB model," *JCAP*, vol. 1012, p. 021, 2010.

[74] A. R. Liddle, "How many cosmological parameters?" *Mon. Not. Roy. Astron. Soc.*, vol. 351, pp. L49–L53, 2004.

[75] T. M. Davis *et al.*, "Scrutinizing Exotic Cosmological Models Using ESSENCE Supernova Data Combined with Other Cosmological Probes," *Astrophys. J.*, vol. 666, pp. 716–725, 2007.

[76] G. Schwarz, "Estimating the dimension of a model," *Ann. Statist.*, vol. 6, no. 2, pp. 461–464, 03 1978. [Online]. Available: http://dx.doi.org/10.1214/aos/1176344136

[77] H. Negishi, K.-i. Nakao, C.-M. Yoo, and R. Nishikawa, "Systematic error due to isotropic inhomogeneities," *Phys. Rev.*, vol. D92, no. 10, p. 103003, 2015.

[78] K. Bolejko, "The effect of inhomogeneities on the distance to the last scattering surface and the accuracy of the CMB analysis," *JCAP*, vol. 1102, p. 025, 2011.

[79] S. Räsänen, "Accelerated expansion from structure formation," *JCAP*, vol. 0611, p. 003, 2006.

[80] T. Buchert and S. Räsänen, "Backreaction in late-time cosmology," *Ann. Rev. Nucl. Part. Sci.*, vol. 62, pp. 57–79, 2012.

[81] T. Buchert *et al.*, "Is there proof that backreaction of inhomogeneities is irrelevant in cosmology?" *Class. Quant. Grav.*, vol. 32, p. 215021, 2015.

[82] J. Adamek, C. Clarkson, R. Durrer, and M. Kunz, "Does small scale structure significantly affect cosmological dynamics?" *Phys. Rev. Lett.*, vol. 114, no. 5, p. 051302, 2015.

[83] D. L. Wiltshire, P. R. Smale, T. Mattsson, and R. Watkins, "Hubble flow variance and the cosmic rest frame," *Phys. Rev.*, vol. D88, p. 083529, 2013.

[84] K. Bolejko, M. A. Nazer, and D. L. Wiltshire, "Differential expansion of space and the Hubble flow anisotropy," *arxiv:1512.07364*, 2015.

[85] T. Delubac *et al.*, "Baryon acoustic oscillations in the Lyα forest of BOSS DR11 quasars," *Astron. Astrophys.*, vol. 574, p. A59, 2015.

[86] A. Font-Ribera *et al.*, "Quasar-Lyman α Forest Cross-Correlation from BOSS DR11 : Baryon Acoustic Oscillations," *JCAP*, vol. 1405, p. 027, 2014.

[87] D. J. Schwarz, C. J. Copi, D. Huterer, and G. D. Starkman, "CMB Anomalies after Planck," 2015. [Online]. Available: http://inspirehep.net/record/1400986/files/arXiv:1510.07929.pdf

[88] C. L. Bennett *et al.*, "First year Wilkinson Microwave Anisotropy Probe (WMAP) observations: Preliminary maps and basic results," *Astrophys. J. Suppl.*, vol. 148, pp. 1–27, 2003.

[89] P. A. R. Ade *et al.*, "Planck 2015 results. XVI. Isotropy and statistics of the CMB," *arxiv:1506.07135*, 2015.

[90] A. de Oliveira-Costa, M. Tegmark, M. Zaldarriaga, and A. Hamilton, "The Significance of the largest scale CMB fluctuations in WMAP," *Phys. Rev.*, vol. D69, p. 063516, 2004.

[91] C. J. Copi, D. Huterer, D. J. Schwarz, and G. D. Starkman, "Large-scale alignments from WMAP and Planck," *Mon. Not. Roy. Astron. Soc.*, vol. 449, no. 4, pp. 3458–3470, 2015.

[92] P. Vielva, E. Martinez-Gonzalez, R. B. Barreiro, J. L. Sanz, and L. Cayon, "Detection of non-Gaussianity in the WMAP 1 - year data using spherical wavelets," *Astrophys. J.*, vol. 609, pp. 22–34, 2004.

[93] M. Cruz, E. Martinez-Gonzalez, P. Vielva, and L. Cayon, "Detection of a non-gaussian spot in WMAP," *Mon. Not. Roy. Astron. Soc.*, vol. 356, pp. 29–40, 2005.

[94] H. Eriksen, F. Hansen, A. Banday, K. Gorski, and P. Lilje, "Asymmetries in the Cosmic Microwave Background anisotropy field," *Astrophys. J.*, vol. 605, pp. 14–20, 2004.

[95] C. Gordon, W. Hu, D. Huterer, and T. M. Crawford, "Spontaneous isotropy breaking: a mechanism for CMB multipole alignments," *Phys. Rev.*, vol. D72, p. 103002, 2005.

[96] T. R. Jaffe, A. J. Banday, H. K. Eriksen, K. M. Gorski, and F. K. Hansen, "Evidence of vorticity and shear at large angular scales in the WMAP data: A Violation of cosmological isotropy?" *Astrophys. J.*, vol. 629, pp. L1–L4, 2005.

[97] J. D. Barrow, R. Juszkiewicz, and D. H. Sonoda, "Universal rotation - How large can it be?" *Mon. Not. Roy. Astron. Soc.*, vol. 213, pp. 917–943, 1985.

[98] T. R. Jaffe, S. Hervik, A. J. Banday, and K. M. Gorski, "On the viability of Bianchi type viih models with dark energy," *Astrophys. J.*, vol. 644, pp. 701–708, 2006.

[99] P. Ade *et al.*, "Planck 2013 results. XXVI. Background geometry and topology of the Universe," *Astron. Astrophys.*, vol. 571, p. A26, 2014.

[100] A. Kovács and J. García-Bellido, "Cosmic troublemakers: the Cold Spot, the Eridanus Supervoid, and the Great Walls," *arxiv:1511.09008*, 2015.

[101] T. S. Koivisto and D. F. Mota, "CMB statistics in noncommutative inflation," *JHEP*, vol. 1102, p. 061, 2011.

[102] J. D. Barrow and S. Hervik, "Simple Types of Anisotropic Inflation," *Phys. Rev.*, vol. D81, p. 023513, 2010.

[103] M. J. Axelsson, F. K. Hansen, T. Koivisto, and D. F. Mota, "Cosmic microwave background anomalies from imperfect dark energy - Confrontation with the data," *Astron. Astrophys.*, vol. 564, p. A113, 2014.

[104] T. Koivisto and D. F. Mota, "Accelerating Cosmologies with an Anisotropic Equation of State," *Astrophys. J.*, vol. 679, pp. 1–5, 2008.

[105] T. S. Koivisto and D. F. Mota, "Anisotropic Dark Energy: Dynamics of Background and Perturbations," *JCAP*, vol. 0806, p. 018, 2008.

[106] L. Perivolaropoulos, "Large Scale Cosmological Anomalies and Inhomogeneous Dark Energy," *Galaxies*, vol. 2, pp. 22–61, 2014.

[107] R. Battye and A. Moss, "Anisotropic dark energy and CMB anomalies," *Phys. Rev.*, vol. D80, p. 023531, 2009.

[108] A. Loeb, "Direct Measurement of Cosmological Parameters from the Cosmic Deceleration of Extragalactic Objects," *Astrophys. J.*, vol. 499, pp. L111–L114, 1998.

[109] J. Liske *et al.*, "Cosmic dynamics in the era of Extremely Large Telescopes," *Mon. Not. Roy. Astron. Soc.*, vol. 386, pp. 1192–1218, 2008.

[110] H.-R. Yu, T.-J. Zhang, and U.-L. Pen, "Method for Direct Measurement of Cosmic Acceleration by 21-cm Absorption Systems," *Phys. Rev. Lett.*, vol. 113, p. 041303, 2014.

[111] A. Sandage, "The Change of Redshift and Apparent Luminosity of Galaxies due to the Deceleration of Selected Expanding Universes." *Astrophys. J.*, vol. 136, p. 319, Sep. 1962.

[112] C.-M. Yoo, T. Kai, and K.-I. Nakao, "Redshift drift in Lemaître-Tolman-Bondi void universes," *Phys. Rev.*, vol. D83, no. 4, p. 043527, Feb. 2011.

[113] C. Hellaby and K. Lake, "Shell crossings and the Tolman model," *Astrophys. J.*, vol. 290, pp. 381–387, Mar. 1985.

[114] A. A. Coley and S. Hervik, "A note on tilted Bianchi type VI_h models: the type III bifurcation," *Class. Quant. Grav.*, vol. 25, no. 19, p. 198001, Oct. 2008.

[115] S. Hervik, R. J. van den Hoogen, W. C. Lim, and A. A. Coley, "Late-time behaviour of the tilted Bianchi type VI(-1/9) models," *Class. Quant. Grav.*, vol. 25, p. 015002, 2008.

[116] S. Hervik and W. C. Lim, "The Late-time behaviour of vortic Bianchi type VIII universes," *Class. Quant. Grav.*, vol. 23, pp. 3017–3035, 2006.

[117] S. Hervik, R. J. van den Hoogen, W. C. Lim, and A. A. Coley, "The Futures of Bianchi type VII0 cosmologies with vorticity," *Class. Quant. Grav.*, vol. 23, pp. 845–866, 2006.

[118] S. Hervik, R. J. van den Hoogen, and A. Coley, "Future asymptotic behaviour of tilted Bianchi models of type IV and VII(h)," *Class. Quant. Grav.*, vol. 22, pp. 607–634, 2005.

[119] S. Hervik, R. J. van den Hoogen, W. C. Lim, and A. A. Coley, "Late-time behaviour of the tilted Bianchi type VIh models," *Class. Quant. Grav.*, vol. 24, pp. 3859–3896, 2007.